Global Modeling of Nitrate and Ammonium: Interaction of Aerosols and Tropospheric Chemistry

Yan Feng and Joyce E. Penner

Department of Atmospheric, Oceanic and Space Sciences, University of Michigan

Abstract. Global radiative forcing of nitrate and ammonium aerosols has mostly been estimated from aerosol concentrations calculated at thermodynamic equilibrium or using approximate treatments for their uptake by aerosols. In this study, a more accurate hybrid dynamical approach (DYN) was used to simulate the uptake of nitrate and ammonium by aerosols and the interaction with tropospheric reactive nitrogen chemistry in a three-dimensional global aerosol and chemistry model, IMPACT, which also treats sulfate, sea salt and mineral dust aerosol. 43% of the global annual average nitrate aerosol burden, 0.16 TgN, and 92% of the global annual average ammonium aerosol burden, 0.29 TgN, exist in the fine mode ($D<1.25\mu m$) that scatters most efficiently. Results from an equilibrium calculation differ significantly from those of DYN since the fraction of fine-mode nitrate to total nitrate (gas plus aerosol) is 9.8%, compared to 13% in DYN. Our results suggest that the estimates of aerosol forcing from equilibrium concentrations will be underestimated. We also show that two common approaches used to treat nitrate and ammonium in aerosol in global models, including the first-order gas-to-particle approximation based on uptake coefficients (UPTAKE) and a hybrid method that combines the former with an equilibrium model (HYB), significantly overpredict the nitrate uptake by aerosols especially that by coarse particles, resulting in total nitrate

aerosol burdens higher than that in DYN by +106% and +47%, respectively. Thus, nitrate aerosol in the coarse mode calculated by HYB is 0.18 Tg N, a factor of 2 more than that in DYN (0.086 Tg N). Excessive formation of the coarse-mode nitrate in HYB leads to near surface nitrate concentrations in the fine mode lower than that in DYN by up to 50% over continents. In addition, near-surface HNO_3 and NO_x concentrations are underpredicted by HYB by up to 90% and 5%, respectively. UPTAKE overpredicts the NO_x burden by 56% and near-surface NO_x concentrations by a factor of 2-5. These results suggest the importance of using the more accurate hybrid dynamical method in the estimates of both aerosol forcing and tropospheric ozone chemistry.

1. Introduction

IPCC [1994] identified nitrate and ammonium as significant anthropogenic sources of aerosol, but there are only a limited number of global model studies of nitrate and ammonium aerosol concentrations [*Adams et al.*, 1999; *Metzger et al.*, 2002; *Liao et al.*, 2003; *Rodriguez and Dabdub*, 2004], and their radiative effects [*van Dorland et al.*, 1997; *Adams et al.*, 2001; *Jacobson*, 2001; *Liao et al.*, 2004]. Nitrate and ammonium aerosol are highly hygroscopic, and can absorb water to form aqueous solutions under typical atmospheric conditions [*Tang and Munkelwitz*, 1994; *ten Brink et al.*, 1996]. So they affect aerosol radiative properties by changing the amount of aerosol water uptake at a given relative humidity, as well as by altering the refractive index of aerosols. Both measurements [*ten Brink et al.*, 1996] and model studies [*van Dorland*, 1997; *Adams et al.*, 2001] have found that nitrate may exert a radiative forcing that is similar to (or even larger than) sulfate aerosols on a regional basis. The relative importance of nitrate versus sulfate aerosol may increase in the future in most industrialized regions of Europe and North America, due to the larger decline of sulfur emissions compared to those of NO_x in the IPCC A2 scenario for year 2100 [*Adams et al.*, 2001]. Recent studies indicate that the condensation of nitric acid on aerosol particles may enhance aerosol activation to cloud droplets by contributing soluble material to the particle surface and elevating the water uptake and growth of aerosol particles [*Kulmala et al.*, 1993, 1995, and 1998; *Goodman et al.*, 2000]. Thus full consideration of aerosol composition including hygroscopic components like nitrate and ammonium is also important in the calculation of aerosol indirect forcing.

The formation of nitrate and ammonium aerosol also strongly affects tropospheric chemistry. Nitrate and ammonium aerosol provide additional particle surfaces for scattering incoming ultra-violet (UV) solar radiation [*Liao et al.*, 2003] and will thus perturb photochemical oxidant production by altering photolysis frequencies. Nitrate aerosol is formed through heterogeneous reactions of nitrogen radicals such as N_2O_5, NO_3, and HNO_3 on aerosol surfaces [*Jacob*, 2000]. During transport in the atmosphere, HNO_3 balances between the gas phase (as nitric acid gas) and the aqueous phase (as nitrate aerosol), determined by its Henry's law coefficient. The presence of nitrate aerosol will affect the rate of conversion of N_2O_5 to HNO_3(g). For example, *Riemer et al.* [2003] found that the presence of nitrate aerosol lowers the reaction probability of the N_2O_5 conversion to HNO_3(g) by one order of magnitude, especially under high-NO_x conditions. Since this conversion was estimated to decrease tropospheric ozone concentrations by 8 – 25% during the winter and 6 – 10% during the summer [*Dentener and Crutzen*, 1993; *Dentener et al.*, 1996; *Tie et al.*, 2003], it is important to account for the presence of nitrate aerosol in computing this rate. The more recent study by *Bauer et al.* [2004] found a global annual mean decrease in tropospheric ozone concentration of 5% with most of the ozone reduction attributed to the uptake of HNO_3 by aerosols. During these heterogeneous processes, ammonium helps to retain nitrate in the aerosol phase by neutralizing the aerosol acidity [*Adams et al.*, 1999].

In order to study the effects of nitrate and ammonium aerosol on radiative processes and gas-phase chemistry, one must first consider the partitioning of semi-volatile nitrate and ammonium between the gas and aerosol phases. Previous global model studies have implemented thermodynamic models into transport models in different ways to

investigate the global concentrations of nitrate and ammonium aerosol [*Adams et al.*, 1999; *Liao et al.*, 2003; *Rodriguez and Dabdue*, 2004]. Several of them estimated the direct forcing of nitrate in aerosols [*Adams et al.*, 2001; *Jacobson*, 2001; *Liao et al.*, 2004], while *Liao et al.* [2003] examined the impact of heterogeneous interactions on tropospheric ozone in a coupled aerosol and chemistry model.

One major limitation of the study reported by *Adams et al.* [1999 and 2001] is that they did not include sea salt and mineral dust aerosols, which are generally coarse particles. Evidence of nitrate in sea salt and mineral dust compounds has been found in both ground-level and free atmosphere measurements [*Wu and Okada*, 1994; *Kerminer et al.*, 1997; *ten Brink et al.*, 1997; *Zhuang et al.*, 1999]. For example, *Yeatman et al.* [2001] found that during polluted continental flow at a costal site, about 40-60% of the nitrate aerosol was present on coarse particles, while under clean marine conditions, almost 100% of aerosol nitrate was converted from small particles to larger particles. Such size-shifting of nitrate also gives rise to a significant fraction of the total aerosol ammonium being on coarse particles (~19-45%). *Jacobson* [2001] used a size-resolved thermodynamic equilibrium model and calculated nitrate and ammonium on sea salt and dust aerosols as well as on sulfate aerosol. However, assuming thermodynamic equilibrium between the gas and aerosol phases may not be appropriate for coarse aerosols in global models. It has been shown [*Meng and Seinfeld*, 1996; *Seinfeld and Pandis*, 1998] that under conditions such as cold temperatures and low aerosol concentrations, the establishment of equilibrium on coarse aerosol particles is only slowly established, with a timescale of the order of several hours or even days. This is longer than the time steps used in chemical transport models (about 1 hour). Departure from the

gas-aerosol equilibrium state has also been observed for coarse aerosols in field studies (e.g., the SCAQS study, *John et al.*, 1989).

Since the most accurate method of solving mass transfer equations dynamically over the whole aerosol size range is computationally very expensive, different approximations have been developed to treat nitrate and ammonium in aerosol for global studies. One approach is to add a mass transport constraint to the equilibrium calculations. In this method, one first calculates the equilibrium concentrations for the gas and bulk-aerosol phases, and then distributes the total aerosol concentrations to different size sections according to a weighting function derived from the mass transfer equation [*Pandis et al.*, 1993]. This method has been applied to describe the distribution of volatile aerosol components in air quality models [*Pandis et al.*, 1993; *Lurmann et al.*, 1997], and *Rodriguez and Dabdub* [2004] implemented it in a global chemistry transport model (IMAGES) to study nitrate and ammonium aerosols. However, this method is still based on the equilibrium assumption. And it neglects differences in the chemical driving forces of each size section on the condensation of volatile species, since it considers aerosols with different size distributions such as sulfate, sea salt and mineral dust, as a bulk aerosol in the thermodynamic treatment within the model. Another treatment of nitrate and ammonium in aerosol was developed and used in *Liao et al.* [2003]. They assumed thermodynamic equilibrium for nitrate and ammonium on sulfate aerosol, and considered the first-order removal of nitrate by dust aerosol, determined by the uptake (or reaction) coefficient of HNO_3 [*Dentener and Crutzen*, 1993]. This method will be evaluated in the next section and further discussed in sensitivity studies (section 4).

In the present study, we calculate the global concentration of nitrate and ammonium aerosol using a more accurate hybrid dynamical approach [*Capaldo et al.*, 2000]. Nitrate and ammonium on sub-micron aerosols (D<1.25 μm) are computed with a gas-aerosol thermodynamic equilibrium model [*Jacobson*, 1999]; for coarse aerosols (D>1.25 μm), the uptake of nitrate and ammonium aerosol is described by dynamic mass transfer calculations.

The following section describes the three-dimensional global aerosol transport model used in this study, and new enhancements to the aerosol model including a simple tropospheric nitrogen chemistry model, a global ammonia cycle model and the interaction of these gases with aerosol. We then present the global distribution of the calculated nitrate and ammonium aerosol concentrations. This is followed by a discussion of the global aerosol budget and comparisons with other studies. Sensitivity studies are performed to demonstrate differences in the concentration and size distribution of nitrate aerosol between using the more accurate hybrid dynamical method and using two approximations. The final section summarizes the major conclusions of this study.

2. Model Description

2.1 Global Aerosol and Chemistry Transport Model

A global aerosol and chemistry transport model, the University of Michigan (UMICH) version of the Lawrence Livermore National Laboratory (LLNL) IMPACT model [*Liu and Penner*, 2002; *Feng et al.*, 2004; *Rotman et al.*, 2004; *Liu et al.*, submitted, 2005], was used as the framework for this study. The spatial resolution of the IMPACT model is 2° latitude by 2.5° longitude in the horizontal, with 26 layers in the vertical from the surface to 0.1 hPa (the mean pressure levels are 994, 971, 930, 875, 813,

745, 675, 605, 537, 472, 410, 353, 302, 258, 220, 187, 158, 133, 112, 94.1, 79.3, 67.0, 56.7, 37.7, 14.3, and 2.64 hPa). For this study, the transport model was driven by assimilated meteorological fields for year 1997, which were available at a 6-hour time interval from the NASA Goddard Data Assimilation Office (DAO) general circulation model (GCM) and interpolated to a 1-hour time interval, the same as the model time step for tracer advection.

The IMPACT model uses a flux-form semi-Lagrangian advection scheme [*Lin and Rood*, 1996]. Dry deposition rates for gases are calculated using a package developed at Harvard University based on the work of *Jacob and Wofsy* [1990], *Wesely* [1989], and *Walcek et al.* [1986]. Dry deposition of aerosol particles uses a resistance-in-series parameterization following *Zhang et al.* [2001]. The wet deposition scavenging parameterization is based on the the Harvard wet scavenging model [*Mari et al.*, 2000; *Liu et al.*, 2001] that is enhanced over previous models [*Giorgi and Chameides*, 1986; *Balkanski et al.*, 1993]. In convective updrafts, the fraction of tracer scavenged is calculated based on the rate constant for conversion of cloud condensate (including liquid and ice) to precipitation (assumed to be 0.005 s^{-1}) and the fraction of tracer present in the cloud condensate f_i (scavenging efficiency). The scavenging efficiency of gases depends on their Henry's law coefficients, except for highly soluble HNO_3 which is assumed to be completely removed. The scavenging efficiencies of sulfate, nitrate, ammonium, and carbonaceous aerosol are 1.0, 1.0, 1.0, and 0.4 in the IMPACT model, respectively. In addition, a first-order washout (in-cloud scavenging of aerosols or gases by cloud or precipitation) and rainout (below-cloud scavenging of aerosols or gases by cloud or precipitation) parameterization is applied for both convective and large-scale

precipitation. The fraction of a tracer lost due to rainout depends on the wet scavenging efficiency of the tracer, the horizontal area-fraction of the grid box experiencing precipitation, and conversion rate of cloud condensate to precipitation. Washout by large-scale precipitation is computed as a first-order loss process using a rate which is calculated by multiplying a constant scavenging efficiency, 0.1 mm^{-1}, by the precipitation rate (in mm hr^{-1}) in the precipitating fraction of the grid box [*Balkaniski et al.*, 1993]. Re-suspension is calculated in any grid box where there is net evaporation of precipitation. A fraction (assumed to be half) or total of the tracer precipitating from above is released in the grid box to reflect the partial or total evaporation of precipitation, respectively. Cumulus transport in the IMPACT model was derived from the relaxed Arakawa-Schubert scheme, as described in detail by *Penner et al.* [1998]. The cumulus mass flux and convective cloud detrainment used in the scheme are derived from the DAO meteorological fields. A full description of the transport and deposition schemes is given in *Rotman et al.* [2004] for the original IMPACT model.

An online sulfur model that predicts the concentrations of SO_2, SO_4^{2-} (represented in 3 aerosol size bins: <0.05 μm, 0.05-0.63 μm, 0.63-1.25 μm in radius), H_2O_2 and DMS was developed for the UMICH version of the IMPACT model [*Liu and Penner*, 2002; *Liu et al.*, submitted, 2005]. This model includes the Global Emissions Inventory Activity (GEIA) emissions of SO_2 and SO_4^{2-} from fossil fuel combustion and industrial activities, SO_2 emissions from biomass burning, aircraft, and non-eruptive volcanoes, as well as an oceanic DMS source. SO_2 is oxidized to SO_4^{2-} in cloud by dissolved O_3 and H_2O_2, and in the gas phase by the OH radical. Both OH and NO_3 radicals oxidize DMS and generate SO_4^{2-}. H_2O_2 is included as a prognostic species, formed from two HO_2 molecules. Three-

dimensional monthly average O_3, OH, and HO_2 concentration fields are taken from a one-year simulation of the chemical transport model GRANTOUR using the climate model CCM1 meteorological fields [*Penner et al.*, 1994]. The diurnal cycle of OH and HO_2 is approximated using the cosine of the solar zenith angle. NO_3 is calculated interactively by a nitrogen chemistry model to be described in the next section. The wet size used in the dry deposition scheme is calculated by the empirical expression of *Gerber* [1985],

$$R_w = \left(\frac{C_1 R_d^{C_2}}{C_3 R_d^{C_4} - LogS} + R_d^3\right)^{\frac{1}{3}}, \quad (1)$$

where R_w and R_d are the wet and dry particle radius, S is the relative humidity expressed as a fraction, and C_1, C_2, C_3, and C_4 are constants whose values are 0.4809, 3.082, 3.110×10^{-11}, and -1.428, respectively. The model yields an average sulfate burden of 0.80 Tg S. This value is intermediate in comparison with other sulfur models that give burdens ranging from 0.53 Tg S [*Chin et al.*, 1996] to 1.05 Tg S [*Lelieveld et al.*, 1997].

Sea salt emissions in the IMPACT model were those provided by *Gong et al.* [1997]. An interpolation was made based on the algorithm of *Monahan et al.* [1986] to derive the size-segregated mass fluxes. Following emission, the sea salt mass is carried in 4 aerosol size bins or sections (0.05-0.63 μm, 0.63-1.25 μm, 1.25-2.5 μm, 2.5-10. μm in radius). The constants C_1, C_2, C_3, and C_4 in the equation (1) which account for the relative humidity dependence of sea salt are 0.7674, 3.079, 2.573×10^{-11}, and -1.424, respectively. The model predicted sea salt burden is about 3.13 Tg. Since most of this mass is associated with coarse particles, sea salt particles are removed mainly by dry deposition.

The dust emission fluxes calculated by *Ginoux et al.* [2001] were interpolated and represented in the same 4 size bins as the sea salt aerosol [*Liu et al.*, 2005, submitted]. Although dust particles may acquire a soluble coating and absorb water, their dry sizes are used in the calculation of the dry deposition velocity since the extent of their water uptake is not well established. For in-cloud scavenging of dust particles, we followed the assumption of *Ginoux et al.* [2001] and completely scavenged dust particles within both convective and large-scale clouds. The model calculated dust burden is about 23.21 Tg. Model estimates of dust burden range from 13.8 Tg by *Takemura et al.* [2000] to 18.7 Tg by *Tegen et al.* [2002], to 31-40 Tg by Ginoux *et al*. [2001]. The large differences between these studies result from large uncertainties in emissions and the different schemes wet and dry deposition schemes used in the models.

A longer description of the aerosol module in the UMICH/IMPACT model and a comparison of the model predicted aerosol concentrations and optical depths with available observations are given in *Liu et al.* [2005, submitted to this journal].

2.2 Nitrogen Chemistry

The gas-phase precursors of nitrate, HNO_3 and N_2O_5, are calculated inline in the IMPACT model with a simple nitrogen chemistry mechanism. The scheme allows 5 tracers to be transported: NO_x ($NO + NO_2$), NO_3, N_2O_5, and HNO_3. Table 1 lists the tropospheric chemical reactions included in the model. The NO_2 concentrations are derived by assuming that photochemical equilibrium is reached between NO and NO_2. Since the reactivity of NO_3 on aerosol surfaces is much smaller than that of N_2O_5 and HNO_3, heterogeneous hydrolysis of NO_3 is neglected in this study. Stratospheric chemistry of gas phase nitrogen is treated more simply. Its sole function is to provide the

proper partitioning between NO_x and $NO_y = HNO_3 + NO_x$ for the stratospheric input at the tropopause. Following *Kraus et al.* [1996], NO_x is converted to HNO_3 everywhere above the tropopause with an e-folding time constant of 13 days. HNO_3 is converted back to NO_2 by photolysis, at varying frequencies up to 3×10^{-7}.

The global fields of OH and O_3 are prescribed as monthly averages as described above. Photolysis frequencies were computed interactively every hour from a look-up table [*Feng et al.*, 2004] that accounts for absorption by O_2 and O_3, Rayleigh scattering, and Mie scattering by clouds and aerosols. Five NO_x sources (emitted as NO_2) were included in this study following *Rotman* et al. [2004]: 21.5 Tg N per year from industrial activities/fossil fuel combustion, 6.4 Tg N per year from biomass burning, 5.0 Tg N per year from lightning, 5.5 Tg N per year from soil processes, and 0.5 Tg N per year from aircraft emissions. Initial stratospheric HNO_3 concentrations were specified, based on model results from a full chemistry version of the UMICH/IMPACT model [*Ito et al.*, 2004 AGU Fall meeting].

The main limitation of this simplified nitrogen chemistry is that it omits organic nitrates. Since organic nitrates form in source regions and transport NO_x to the remote troposphere, this omission may result in overpredicted NO_x and HNO_3 concentrations in source regions and underpredicted NO_x and HNO_3 concentrations in the remote troposphere [e.g., *Singh et al.*, 1998 and 2000; *Schultz et al.*, 1999].

For nitric acid (HNO_3), the effective Henry's law constant used in the dry deposition scheme is 3.17×10^{11} M atm^{-1} at pH = 5. The size-dependent dry deposition of nitrate aerosol used the effective radius for the dominant aerosol type in each size section. Thus the dry deposition of nitrate in the size section, r = 0.01 – 0.63 μm (bin 1) was treated the

same as sulfate, while that in the size range from 0.63 – 2.5 μm (bins 2 and 3) was treated the same as sea salt, and that in the range 2.5 – 10 μm (bin 4), was treated the same as dust aerosol. The wet scavenging efficiency for nitrate aerosol was set equal to that for sulfate aerosol.

2.3 Ammonia Cycle

The ammonia cycle was simulated by adding two tracers: ammonium (NH_4^+) and its gas-phase precursor ammonia (NH_3) in the IMPACT model. Ammonia emissions were taken from the global inventory of *Bouwman et al.* [1997]. The total ammonia source included in this inventory is estimated to be 54 Tg N per year, and Table 2 lists the contributions from individual sources. The fact that fertilizer related activities contribute most to the ammonia emissions implies that agricultural regions tend to have the highest ammonia emissions. Figure 1 shows the geographic distribution of the NH_3 emissions. The strongest source regions occur in eastern China, India, Europe, the American Midwest, and southern Brazil. The total emissions estimate of this inventory is higher than the 45 Tg N per year used by *Dentener and Crutzen* [1994] in their model of the ammonia cycle, lower than the 75 Tg N per year estimate of *Schlesinger and Hartley* [1992], and almost the same as the 54 Tg N per year estimate of *Warneck* [1988]. Although some sources, for example, those from crops, fertilizer, and animal waste, likely exhibit seasonal differences depending on the crop production cycle and temperature, their monthly variations are not available in the current ammonia inventory. In the absence of more detailed information, the annual average emission fluxes from all the sources were used for this study.

Ammonia (NH_3) undergoes one reaction in the atmosphere with the OH radical [*DeMore et al.*, 1997],

$$NH_3 + OH \rightarrow NH_2 + H_2O \quad (2)$$

We did not include this reaction for this study, since it only plays an insignificant role in the global ammonia budget [*Adams et al.*, 1999]. For wet deposition of NH_3, we use an effective Henry's law coefficient of 1.05×10^6 M atm^{-1} at pH = 5. Aerosol ammonium was treated similarly to nitrate aerosol in the dry and wet deposition schemes.

2.4 Heterogeneous Interaction of Aerosols and Gas-phase Chemistry

Aerosol particles are frequently found as internal mixtures with multiple components including sulfate, sea salt, nitrate and dust compounds [*Okada et al.*, 1990; *Fan et al.*, 1996; *Zhou et al.*, 1996; *Niimura et al.*, 1998; *Yamato and Tanaka*, 1994; *Zhang et al.*, 2003], probably due to large-scale condensation and coagulation processes. Therefore, sulfate, sea salt and mineral dust aerosols were assumed to be internally mixed. Organic aerosol compounds may contribute to a large fraction of total aerosol mass; however, little is known about their composition and hygroscopic properties. Although a range of water-soluble organic compounds have been identified in the atmosphere [*Saxena and Hildemann*, 1996], a better characterization of the organic components of the aerosol is needed in order to characterize their water uptake and interaction with other compounds. Therefore, we did not consider the formation of nitrate and ammonium on organic aerosols. Similarly, black carbon was not considered, since it is unlikely to be hydrated except in association with organics and other compounds.

The chemical composition of sea salt aerosol is assumed to be 100% of NaCl. Dust aerosols generally consist of insoluble metal oxides and a small fraction of alkaline

components. The alkalinity of dust is to a great extent determined by the calcium carbonate ($CaCO_3$) content. It varies with the source region of the dust aerosol and may be modified by other pollutants during long-distance transport. In this study, mineral dust aerosol is assumed to be: 7% $CaCO_3$, 5.5% $MgCO_3$, 3.3% K_2CO_3, 2.6% Na_2CO_3, 60% SiO_2, 14.1% Al_2O_3 and 6.9% Fe_2O_3 [*Gillette et al.*, 1993]. This gives an average of Ca^{2+} content of 4.2%, which is somewhat larger than the global average crustal Ca content of 3.6% given by *Jaenicke* [1988], but smaller than the value of 5% used by most previous model studies [*Dentener et al.*, 1996; *Liao et al.*, 2003] which considered only Ca^{2+} for the alkaline material in dust aerosol. Heterogeneous reactions included in the model are also shown in Table 1.

The heterogeneous uptake of nitrate and ammonium by aerosol mixtures is modeled in the UMICH/IMPACT model using a hybrid dynamical approach. With this method, the thermodynamic equilibrium model [*Jacobson*, 1999] is applied to aerosols in size bin 1 ($D<1.25\mu m$) (hereafter referred to as the fine mode); while the gas and aerosol concentrations are determined by dynamically solving mass transfer equations for particles in the other 3 bins ($D>1.25\mu m$) (hereafter referred to as the coarse mode), Since the mass transport of gases is considered only for super-micron aerosols, the computational intensity of integrating the mass transfer equations is lessened. *Capaldo et al.* [2000] applied a similar approach in an air pollution model, and they found that this method maintained most of the predictive capability of dynamically solving mass transfer equations over the entire aerosol size range, and was 50 times more computationally efficient in their test cases.

Wexler and Seinfeld [1990] and *Dassios and Pandis* [1999] calculated the equilibrium time constants for ammonium nitrate aerosol and indicated that particles with diameter less than 1μm generally have equilibrium time scales of the order of a few minutes under typical atmospheric conditions. Since our transport model time step is one hour and the equilibrium time scale depends mostly on particle size, the equilibrium assumption is well justified for aerosols in the fine mode. Moreover, the chemical composition is also quite similar for aerosols in this size range: for continental aerosols, they are mainly composed of sulfate, ammonium, and nitrate; over the oceans, the main component is sea salt. Therefore, the chemical driving force among particles within this size section is similar and there is no need to use a finer division of bins in this size range.

The partitioning of nitrate and ammonium in the other 3 size bins is described by mass transfer equations,

$$\begin{cases} \dfrac{dC_{\infty}}{dt} = -\sum_{i}^{n} k_i (C_{\infty} - C_{i,eq}) \\ \dfrac{dC_i}{dt} = k_i (C_{\infty} - C_{i,eq}) \\ k_i = 4\pi D_g r_i n_i \dfrac{0.75\,\alpha\,(1 + Kn_i)}{Kn_i^2 + Kn_i + 0.283\,Kn_i\alpha + 0.75\,\alpha} \end{cases} \tag{3}$$

where D_g is the diffusivity, r_i is the radius of particles in size bin i, n_i is the aerosol number concentration, C_{∞} is the ambient gas-phase concentration (moles per m^3 of air) and C_i is the aqueous-phase concentration. $C_{i,eq}$ is the equilibrium vapor concentration on the particle surface, which is calculated with the thermodynamic equilibrium model based on the aerosol composition of each size bin. The formulation of the mass transfer coefficient k_i is based on the solution of *Fuchs and Sutugin* [1971], where Kn_i is the Knudsen number, and the accommodation coefficient (α) represents the sticking probability of a vapor molecule at the surface of a particle. We used 0.193, 0.092, and 0.1

for the accommodation coefficients of HNO_3, NH_3, and N_2O_5 on aerosols, respectively, based on measurements at 298 K by *Van Doren* [1990 and 1991]. These values for α are at the upper end of the corresponding uptake coefficients (γ) used in the literature, satisfying the general relationship $\gamma \leq \alpha$. Equations (3) were integrated over the model time step (1 hour) and were solved simultaneously for aerosol nitrate (NO_3^-) and aerosol ammonium (NH_4^+) concentrations in each of the 3 aerosol bins of the coarse mode as well as for concentrations of their gaseous precursors, HNO_3(g) and NH_3(g).

This hybrid dynamical method should be more accurate than a thermodynamic equilibrium model. It considers the diffusion constraint in the mass transport from the gas phase to particles, which frequently causes coarse aerosols to be in a non-equilibrium state. This method is also better than the first-order removal approximation in which the removal rate K is usually defined as [*Schwartz*, 1986],

$$K = \left(\frac{r}{D_g} + \frac{4}{\upsilon\gamma}\right)^{-1} A \tag{4}$$

where r is the aerosol radius, A is the aerosol surface area, D_g (cm^2 s^{-1}) is the gas phase diffusion coefficient, and υ is the mean molecular speed (cm s^{-1}). γ is the uptake coefficient, which is the ratio of the number of gaseous molecules entering the particle over the number of molecules colliding with the surface. Compared to the mass transfer equation (equation (3)), equation (4) does not explicitly include the equilibrium vapor concentration of species on particle surfaces ($C_{i,eq}$), which depends on the ambient relative humidity, temperature, and the immediate aerosol chemical composition during the gas-to-aerosol diffusion. Instead, the dependence of the mass transfer rate on $C_{i,eq}$ is approximately represented in uptake coefficients measured under certain laboratory

conditions. Use of these uptake coefficients can significantly affect the results of global model studies. For example, *Bauer et al.* [2004] found that with the upper limit for γ_{N2O5} (0.02), tropospheric ozone mass is decreased by 0.8%; with the lower limit of γ_{N2O5} (0.003), the reaction has almost no impact on ozone concentrations. They also found that lowering the uptake coefficient of HNO_3 by two orders of magnitude from 0.1 to 0.001 resulted in a much smaller decrease of tropospheric ozone, from 4.5% to 2.2%. This suggests that the calculation of tropospheric ozone concentrations is sensitive to the processes approximated by uptake coefficients, and that the first-order removal approximation, which only considers the diffusion dependence on particle size, could introduce inaccuracies in global results. With the hybrid dynamical method, the mass transfer equation (3) considers both the diffusion constraint (represented by k_i) and the chemistry constraint (represented by $C_{i,eq}$), and calculates mass transfer rates dynamically for coarse aerosols.

Figure 2 shows a schematic of the integration of the hybrid dynamic approach into the global aerosol and chemistry transport model, UMICH/IMPACT. The integrated model was run for a period of four simulation months: January, April, July and October, to obtain a representation of the annual average of the global concentrations of nitrate and ammonium aerosol. A two-month spin-up time for January plus another for July was used to generate background values as initial concentrations for the production run. The global model requires 3 days of CPU time on 64 IBM SP3 processors (~1.5 GB) to complete a one-month simulation.

3. Global Results

3.1 Nitrate Aerosol

The simulated monthly averaged concentrations of fine and coarse mode nitrate aerosol in the lowest 3 layers of the model are shown in Figure 3 for January and July. In January, fine-mode nitrate mixing ratios exceeding 1 ppbv occur in Europe, eastern China, and the eastern US. Due to the absence of sea salt and mineral dust aerosol over these regions, nitrate aerosol exists mainly as neutralized ammonium nitrate, in an amount which is determined by thermodynamic equilibrium. In July, the increase of sulfate aerosol in the northern hemisphere due to the enhanced oxidation of SO_2 reduces the fine-mode nitrate formation significantly, because ammonia reacts preferentially with sulfate. Other localized source regions of NO_x such as portions of the South America and South Africa, also have high concentrations of fine-mode nitrate aerosol, from 100 pptv to 1 ppbv. There are lower nitrate aerosol concentrations in the summer hemisphere, because nitrate preferentially stays in the gas phase under high temperatures. In addition, large areas with a significant amount of the fine-mode nitrate concentrations (over 300 ppt) are present at high latitudes (> 50°N) in the northern hemisphere in January. This nitrate is formed primarily through the hydrolysis of N_2O_5 on the surface of sulfate aerosols under low temperatures at night. This heterogeneous production of nitrate is not that important in July due to the rapid photolysis and thermal decomposition of N_2O_5. Marine concentrations of the fine-mode nitrate aerosol are negligible, less than 100 pptv almost everywhere.

Coarse-mode nitrate aerosol concentrations exceeding 1 ppbv are predicted near the surface in dust source regions including Central Africa, the Asian and Australian deserts. Biomass burning areas in Central Africa have the largest coarse-mode nitrate concentrations, up to 3 ppbv in January. When the nitrogen sources from biomass

burning shift southward in July, nitrate mixing ratios in Central Africa are reduced to 300 pptv or so. Nitrate in the coarse mode over the Asian dust region increases from 300 - 1000 pptv in January to 1000 - 3000 pptv in July as a result of the larger dust fluxes occurring in June - July in this region. Marine concentrations of coarse-mode nitrate are over 30 pptv in general. They are larger than the concentrations of nitrate in the fine mode, because most of the sea salt mass is associated with coarse particles. The global mean fine-mode nitrate aerosol mixing ratio is 233 pptv near the surface in January, which is a factor of 2 larger than that of the predicted coarse-mode nitrate aerosol (104 pptv). In July, the global mean fine-mode nitrate aerosol mixing ratio is 28 pptv, only 1/3 of that of the coarse-mode nitrate (86 pptv).

Figure 4 shows the fraction of nitrate aerosol in the fine mode in the lowest 3 layers of the model in January and July, respectively. At locations close to deserts, less than 10% of nitrate aerosol is associated with fine-mode particles throughout the year. In July, the fine-mode nitrate contributes less than 50% of the nitrate aerosol except for the most polluted regions over continents. These results are consistent with those of *Liao et al.* [2003] who found that there is more nitrate on dust aerosol (which are mostly coarse particles) than on non-dust aerosol. In contrast, however, *Rodriguez and Dabdub* [2004] estimated that over 80% of the near-surface nitrate aerosol was associated with fine-mode particles over most regions. Our results differ from those of *Rodriguez and Dabdub* [2004] because they used a derived weighting function to allocate nitrate and ammonium aerosol to different size sections, which tends to excessively favor small particles. This method could potentially lead to a significant overestimation of the direct radiative forcing of nitrate.

Figure 5 shows the fraction of total nitrate occurring as aerosol near the surface in January and July (i.e. $[NO_3^-] / [NO_3^- + HNO_3(g)]$). For both months, nitrate formed on coarse particles governs the distribution of the large fractions of aerosol nitrate to total nitrate over most regions. At locations with high concentrations of sea salt or dust aerosol, more than 50% of total nitrate is in the aerosol phase. Aerosol nitrate fractions over the Asian deserts, the Arabian Peninsula, the Saharan deserts, and an extended area over the North Atlantic, approach to 100%. In these regions, the partitioning of nitrate into aerosol is limited only by the availability of nitric acid.

The annual and zonal average $HNO_3(g)$ and nitrate aerosol (NO_3^-) mixing ratios are shown in Figure 6. The largest nitrate aerosol concentrations (over 500 pptv) occur at mid-latitudes in the Northern Hemisphere near the surface and drop rapidly towards the Southern Hemisphere and as altitude increases. The concentrations of $HNO_3(g)$ decrease less dramatically than nitrate aerosol with increasing altitude due to the production of $HNO_3(g)$ from NO_x sources in the free atmosphere. $HNO_3(g)$ mixing ratios exceed 200 pptv in the middle and upper troposphere north of 30°S.

3.2 Ammonium Aerosol

Predicted monthly average mixing ratios of ammonium aerosol, for $D<1.25$ μm and $D>1.25$ μm, are shown in Figure 7 for January and July. The highest ammonium mixing ratios, over 3 ppbv, are found in agricultural or industrialized areas, such as the eastern US, Europe, and China. Biomass burning areas in South America and South Africa also have high concentrations of ammonium, about 1 ppbv. Less than 10% of the total ammonium aerosol is found on coarse particles over most regions, except for the Sahel region where the fraction of coarse-mode ammonium aerosol exceeds 50%. In general,

the alkaline compounds of sea salt and dust aerosol make it difficult for $NH_3(g)$ to partition into coarse particles; on the other hand, biomass burning over the Sahel region produces a significant amount of nitric acid, which is able to neutralize the alkalinity of dust aerosol, so that ammonium nitrate can form on these coarse particles. The mixing ratios of ammonium aerosol generally exceed 300 pptv over the remote continents.

Figure 8 shows the molar ratio of ammonium aerosol to sulfate aerosol (NH_4^+/SO_4^{2-}) in the lowest 3 model layers in January and July. Most of the current global aerosol models assume that ammonium aerosol is present on sulfate aerosol with a molar ratio to sulfate of 2. While this assumption is probably good for remote continental areas, Figure 8 shows that there are much higher molar ratios of ammonium to sulfate in polluted regions due to the presence of aerosol nitrate, especially in the Northern Hemisphere in January (exceeding 10:1 in Europe). Therefore, the assumption of a constant molar ratio of 2 for NH_4^+/SO_4^{2-} could significantly bias the forcing by anthropogenic aerosols in global models.

The fraction of ammonia occurring in the aerosol phase in the lowest 3 layers of the model is shown in Figure 9. Throughout the boundary layer (from 994 - 930 hPa), over 50% of total ammonia partitions into the aerosol phase over continental polluted regions with as much as 100% at high latitudes. The aerosol-phase ammonium has a longer residence time in the atmosphere than gas-phase ammonia, so it plays a key role in determining the pH values of cloud condensation nuclei and precipitation.

Annual and zonal average ammonia and ammonium aerosol mixing ratios are shown in Figure 10. In contrast to $HNO_3(g)$ and nitrate aerosol, ammonia concentrations decrease more rapidly than those of ammonium aerosol from the surface to high altitudes.

This is mainly because there are no additional NH_3(g) sources available in the free atmosphere, and all of the available NH_3(g) is emitted from surface sources. Moreover, the lower temperatures at high altitudes make it easier to condense ammonia on sulfate aerosol, which partly compensates for the decrease of the available particles with altitude. Above 500 hPa, almost 100% of NH_3(g) is converted to NH_4^+ aerosol.

The modeled and observed surface concentrations of sulfate, nitrate and ammonium aerosols were compared with ground-based measurement data over both oceans and polluted continental regions, and the agreement generally falls within a factor of 2 [*Feng, Y.*, Ph.D. thesis, 2005].

3.4 Global Budgets and Comparison with Other Studies

The global budgets of nitrate and ammonium aerosol and their net mass conversion rates to/from their gaseous precursors are summarized in Figure 11. All of the annual budget components such as burden, deposition fluxes etc., were estimated based on the average of the January, April, July and October results. In addition, the comparison of the global budgets in this work with several other studies is summarized in Table 3.

As shown in Figure 11, the tropospheric burden of HNO_3 (gaseous precursor of nitrate aerosol) is computed to be 0.37 Tg N (accumulated for levels below 200 hPa). The net chemical production of HNO_3 from gas-phase chemistry plus heterogeneous conversion from N_2O_5 on aerosols is 35.8 Tg N yr^{-1}, which is about 92% of the total NO_x emissions (38.9 Tg N yr^{-1}). This HNO_3 production is larger than the 29.7 Tg N yr^{-1} given by *Rodriguez and Dabdub* [2004] (hereafter referred to as RD04) and the 28.1 Tg N yr^{-1} given by *Liao et al.* [2004] (hereafter referred to as L04) with their NO_x emissions, 34.7 and 40. Tg N yr^{-1}, respectively, as shown in Table 3. The conversion of HNO_3 to aerosol

NO_3^- is 11.6 Tg N yr^{-1} in this study, which is about 32% of the total HNO_3 removal, and is lower than that of R04 (19.8 Tg N yr^{-1}) and L04 (13.6 Tg N yr^{-1}).

The nitrate aerosol burden predicted here (0.16 Tg N) is slightly lower than the 0.18 Tg N given by L04, but both are much less than that of R04 (0.42 Tg N). We calculate a nitrate aerosol lifetime of 5 days, which is shorter than the 7.7 days calculated by RD04, but comparable to the lifetime calculated by L04 (4.9 days). By neglecting the time needed to achieve gas-aerosol equilibrium, RD04 may have significantly overestimated the nitrate aerosol burden, especially that in the coarse mode. According to L04, 65% of nitrate aerosol was formed on dust aerosol, mostly coarse particles. They also estimated that 30% of the non-dust nitrate was associated with sea salt aerosol on a global average basis. This means that L04 predicted that roughly 72% (= 65%+35%×30%×71%) of nitrate aerosol was in the coarse mode, if we assume that 71% of the sea salt aerosol (mass) is in the coarse [*Quinn et al.,* 1998]. This is significantly higher than the coarse fraction of nitrate aerosol obtained in this study, which is 57%. We will further examine the method used by L04 for nitrate uptake in the sensitivity studies of next section.

Table 3 also shows that there are large differences in the amount of dry and wet deposition of nitrate aerosol between different global model studies. R04 removed nitrate aerosol through wet deposition predominantly, while dry deposition of nitrate aerosol is more efficient than wet deposition in L04. Our total deposition is similar to that of L04, but 74% is through wet deposition compared to their 43%. One of reasons for these differences is because different model treatments for nitrate in aerosol result in nitrate being on different particle sizes, and nitrate on coarse particles is removed more efficiently by dry deposition while nitrate on fine particles is removed mainly through

wet deposition. The ratio between nitrate aerosol dry and wet deposition is important because it plays a significant role in determining the global distribution of nitrogen deposition in the atmosphere, which may affect the global carbon cycle in the biosphere.

The global budget of nitrate in Figure 11 also suggests an important link to tropospheric ozone chemistry. Most of the current global gas-phase chemistry models only consider the heterogeneous conversion of N_2O_5 to HNO_3 on aerosols [e.g., *Dentener and Crutzen*, 1993; *Dentener et al.*, 1996; *Tie et al.*, 2001]. Since the formation of aerosol nitrate removes HNO_3, it could further enhance the decrease of tropospheric ozone due to the loss of NO_x through this heterogeneous reaction. In this study, the calculated nitrate aerosol burden (0.16 Tg N) is about 43% of the HNO_3 burden (0.37 Tg N) on a global and annual average basis. This means that the conversion of HNO_3 to NO_x is probably reduced by 43% when nitrate aerosol formation is included. The recycling of NO_x from HNO_3 (4.8 Tg N yr^{-1}) is about 12% of the tropospheric NO_x emissions (38.9 Tg N yr^{-1}), thus the omission of nitrate aerosol will underestimate the NO_x loss rate due to heterogeneous reactions by 5% and overpredict the tropospheric ozone concentrations. The impact on tropospheric nitrogen oxides and ozone may be more significant regionally. In addition to *Liao et al.* [2003], *Bauer et al.* [2004] also studied the effect of the heterogeneous uptake of HNO_3 by aerosols on tropospheric ozone. In next section, we will also examine the approach used by *Bauer et al.* [2004] for nitrate uptake and compare it with the more accurate hybrid dynamical method used here.

For ammonia, nearly half of its 54.1 Tg N emissions per year are taken up by aerosols, with about 92% of them in the fine-mode, as shown in Figure 11. While NH_3 is removed more efficiently by dry deposition, 89% of the aerosol NH_4^+ is removed by wet

deposition. The lifetime of aerosol NH_4^+, 4.1 days, is much longer than that of NH_3, 0.57 days. Our NH_4^+ lifetime is similar to that calculated by RD04 (3.6 days) and *Adams et al.* [1999] (hereafter referred as A99) (4.2 days), as shown in Table 3. The omission of sea salt and dust aerosol in A99 only resulted a slightly longer lifetime and larger burden for aerosol NH_4^+, since NH_4^+ is mainly taken up by sulfate aerosol in the fine mode. However, the NH_3 lifetime given by A99 (0.93 days) and RD04 (1.4) days are both much longer than that in this study (0.57 days). The larger NH_3 wet deposition in this study may be the major reason for our shorter lifetime, although the effective Henry's law constant for NH_3 that we used in the wet deposition scheme (1.05×10^6 M atm^{-1}) is even smaller than the value used in A99 (3.3×10^6 M atm^{-1}). Our wet deposition scheme for gases and the precipitation rates from the assimilated meteorology data are expected to lead to different results from the GCM wet deposition treatment and precipitation used in A99, however, a more detailed analysis is beyond the scope of this work. To compare with RD04, their equilibrium assumption limited the NH_4^+ production to only 4.5 Tg N yr^{-1}, which is less than 1/5 of that in our prediction. Because the alkaline compounds in sea salt and dust aerosol are all available to compete for nitrate with no consideration of mass transport limitation in RD04, less nitrate is left to neutralize the ammonium. This causes a much lower conversion of NH_3 to NH_4^+ in RD04 and a much longer lifetime for NH_3 than that in this study.

4. Sensitivity Studies

Figure 12 shows the fraction of total nitrate that is in the fine and coarse aerosol modes derived from global calculations with a thermodynamic equilibrium model. These results were calculated offline at each grid cell (5°×7.5° horizontally and 14 vertical

levels) based on three-dimensional monthly average gaseous (NH_3 and HNO_3) and aerosol (sulfate, sea salt and mineral dust) concentrations which were generated from chemical transport model simulations [*Dentener and Crutzen*, 1994; *Penner et al.*, 1994; *Chuang et al.*, 1997; *Penner et al.*, 2001], with monthly averaged relative humidities [ECHAM4, *Roeckner et al.*, 1996] and temperatures [CCM1, *Williamson et al.*, 1987]. The two-month average results for January and July are shown. This equilibrium calculation predicted that 41% of the total nitrate occurred as nitrate aerosol and that only 25% of the total aerosol nitrate was on fine-mode particles. If sea salt and mineral dust is excluded, the equilibrium model calculated that 10% of total nitrate existed in the aerosol phase, all of which was in the fine mode. This test shows that a significant part of nitrate aerosol is formed on sea salt and mineral dust aerosol at thermodynamic equilibrium. Despite differences in model conditions, the UMICH/IMPACT model implemented with the hybrid dynamical method predicted a lower fraction of nitrate in aerosol (30%) and a higher fraction of nitrate in the fine mode (43%), relative to the equilibrium calculations. Nitrate fraction in the most scattering-efficient size range to total nitrate is increased from 9.8% in the equilibrium calculation to 13% with the hybrid dynamical treatment. This comparison suggests that the equilibrium assumption leads to a substantial uptake of nitrate by aerosol, mainly by coarse particles. As a result, it underpredicts nitrate aerosol in the fine mode to a large extent.

In addition to the equilibrium model, two commonly used approximate treatments for aerosol nitrate in global models were also examined: the first-order removal approximation based on uptake coefficients (hereafter referred to as UPTAKE) and a hybrid approach (hereafter referred to as HYB), which adopts the UPTAKE method for

nitrate uptake by dust aerosol and assumed gas-aerosol equilibrium on either sulfate aerosols [*Liao et al.*, 2003] or sulfate and sea salt aerosols [*Liao et al.,* 2004]. Like *Bauer et al.* [2004], we only considered heterogeneous reactions on dust aerosol in the UPTAKE sensitivity study. Previous studies such as *Dentener and Crutzen* [1993] and *Tie et al.* [2003] also applied this approach to the heterogeneous conversion from N_2O_5 to HNO_3 on sulfate and/or sea salt aerosols, but it can not be used to treat the conversion of HNO_3 to nitrate aerosol. Because most of the sulfate mass is in the fine mode, the mass transport from the gas to the aerosol phase is fast and the formation of nitrate on sulfate aerosol is therefore mainly constrained by the acidity of the aerosol solution which is determined by the availability of ammonium in the aerosol. Therefore, the UPTAKE approximation would significantly overpredict nitrate on sulfate aerosol. In a test run using UPTAKE on sea salt aerosol, we also obtained an unrealistically significant increase in aerosol nitrate using the UPTAKE method. An equilibrium assumption was made in *Liao et al.* [2004] for nitrate uptake by sea salt aerosol, but it also does not seem appropriate since sea salt is still mainly in the coarse mode. Therefore, we considered only sulfate and dust aerosol in the HYB sensitivity study, as in *Liao et al.* [2003]. We further assumed that no nitrate uptake by dust could occur if the total moles of aerosol nitrate exceed those of the available alkaline compounds in dust. The uptake coefficients used for HNO_3 and N_2O_5 were 0.1 and 0.05, respectively, the same as those in *Bauer et al.* [2004] and *Liao et al.* [2003]. Table 4 summarizes the aerosol types considered in the base case (DYN) and the sensitivity studies (UPTAKE and HYB), and compares the nitrate global budgets obtained in each case. The results for the averages of January and July are shown.

4.1 Effects on HNO_3 and NO_x

As shown in Table 4, both UPTAKE and HYB predicted lower HNO_3 burdens in the troposphere (i.e., 0.20 and 0.31 Tg N, respectively, compared to 0.38 Tg N in DYN), and higher nitrate aerosol burden, (i.e., 0.35 and 0.25 Tg N, respectively, compared to 0.17 Tg N in DYN). The UPTAKE and DYN methods overestimate nitrate in the aerosol phase by 106% and 47%, respectively. Heterogeneous conversion of N_2O_5 to HNO_3 calculated by UPTAKE is the lowest of the three methods, only 4.5 Tg N yr^{-1}. This is mainly because sulfate aerosol is not treated in UPTAKE. The inclusion of sulfate aerosol in DYN and HYB provides additional large reactive surfaces for N_2O_5 conversion. The absence of sulfate aerosol does not prevent the fact that UPTAKE calculates a larger formation of aerosol nitrate (NO_3^-) from HNO_3, 20.7 Tg N yr^{-1}, than does DYN (12.6 Tg N yr^{-1}). This overestimation by UPTAKE occurs mainly on dust aerosols in the coarse mode. HYB also overpredicts the nitrate aerosol formation but to a lesser extent, because it inserts an upper limit for the uptake of nitrate determined by the available alkalinity of the dust. The net heterogeneous production of HNO_3 is 3.5 and 0.7 Tg N yr^{-1} in DYN and HYB, respectively, while a net heterogeneous loss of HNO_3, 16.2 Tg N yr^{-1}, is predicted by UPTAKE. Since the conversion of N_2O_5 to HNO_3 removes tropospheric NO_x, underestimates by UPTAKE lead to a higher NO_x burden (0.42 Tg) than in DYN (0.27 Tg), although it significantly overpredicts the uptake of nitrate by aerosols. As a result, the decrease of tropospheric ozone concentrations due to heterogeneous interactions is probably underestimated in model studies using the UPTAKE method, such as *Bauer et al.* [2004]. With HYB, the large overestimation of nitrate aerosol formation reduces HNO_3 concentrations but has little impact on the tropospheric NO_x burden.

Figure 13 shows the geographic distribution of HNO_3 and NO_x concentrations calculated by DYN in the lowest 3 layers of the model. Also shown are the ratios of HNO_3 and NO_x concentrations calculated by UPTAKE and HYB to those of DYN. NO_x source regions such as industrialized areas in the Northern Hemisphere and biomass burning areas in the Southern Hemisphere also exhibit high HNO_3 concentrations. In addition, since HNO_3 is transported further than NO_x, its concentrations over the remote continents and oceans exceed 30-100 pptv. The ratios of HNO_3 in UPTAKE and HYB to those in DYN are as low as 0.1 over the Arabian Peninsula, portions of the Central African deserts and the Australian deserts. Without sulfate aerosol, UPTAKE underpredicts HNO_3 concentrations relative to DYN by a factor of 2 more than HYB does, especially at mid- and high latitudes in the Northern Hemisphere. Both UPTAKE and HYB predict higher HNO_3 concentrations than DYN over small areas in Central Africa where HNO_3(g) concentrations are less than 10 ppbv and nitrate is mainly in the aerosol phase. This is due to the extremely high dust concentrations over these regions which result in very low surface concentrations of HNO_3. The mass transport of HNO_3 to aerosols calculated with DYN is thus determined by the HNO_3 accommodation coefficient (0.19) in the model. This leads to a more efficient removal of HNO_3 by DYN, because UPTAKE and HYB use a smaller uptake coefficient (0.1) for the uptake of HNO_3 by aerosols. The HNO_3 ratios are larger than 1 over the oceans in HYB and UPTAKE, since they do not include the uptake of nitrate by sea salt aerosol as DYN does. The surface NOx concentrations are overpredicted by UPTAKE by as much as 2 to 5 times than that of DYN over NO_x source regions, where they are only underestimated by HYB by less than 5%.

4.2 Effects on Nitrate Aerosol Size Distribution

The magnitude of direct forcing by nitrate aerosol is mainly determined by the amount of nitrate in the fine mode that is radiatively important. The coarse-mode nitrate may be important in the calculation of indirect effects of aerosol through the alteration of the highest saturation relative humidity in aerosol activation to cloud droplets. As shown in Table 4, HYB calculates a nitrate aerosol burden in the fine mode (0.075 Tg N) that is similar to that calculated by DYN (0.079 Tg N). However, as shown in Figure 14, the geographic distribution of fine mode nitrate in HYB is not the same as that in DYN.

The nitrate aerosol burden in the coarse mode computed by HYB (0.18 Tg N) is 2 times larger than that of DYN (0.086 Tg N). Figure 14 shows the geographic distribution of aerosol nitrate (NO_3^-) concentrations in the two modes calculated by DYN and the ratios of NO_3^- concentrations between HYB and DYN in these modes in the lowest 3 layers of the model. Aerosol nitrate concentrations in the coarse mode are overestimated by HYB over most of the model domain up to 6 times, compared to DYN. These overestimates are due to excessive uptake by dust aerosol, because HYB does not account for the interactive calculation of HNO_3 during the mass transport of HNO_3 to the aerosol surface. Thus, assuming an HNO_3 uptake coefficient of 0.1 is generally too large. There is a less significant overprediction in HYB in major desert regions because HYB does not allow further uptake of nitrate after nitrate on dust aerosol exceeds the amount of alkaline compounds in the dust. We note that higher surface HNO_3(g) concentrations are predicted by HYB in a very small region of Central Africa (shown in Figure 13), but this does not lead to higher nitrate concentrations in HYB because nitrate in the aerosol size range from 0.63 to 2.5 μm (bins 2 and 3) is removed more efficiently by dry deposition in

DYN (since DYN uses the same relative humidity growth as sea salt in these size bins) than in HYB (where the relative humidity growth is assumed to be the same as dust). Nevertheless, the region affected by this phenomena is very small and the HNO_3(g) gas concentrations are also small.

As noted above, the fine mode aerosol nitrate in HYB is distributed differently than in DYN. This is because in establishing equilibrium between the gas phase and the aerosol phase, nitrate may evaporate from the fine mode to compensate for the excessive uptake in the coarse mode. Therefore, HYB generally predicts lower nitrate concentrations in the fine mode over remote continents by as much as low as 10%. Nevertheless, because HYB assumes only ammonium sulfate and ammonium nitrate aerosol in the fine mode, it predicts higher nitrate concentrations (by up to 50%) in sulfate source regions compared to DYN because DYN assumes an ammonium sulfate, ammonium nitrate and dust aerosol mixture in the fine mode. Thus, some of the sulfate has formed compounds associated with dust in DYN. Over the oceans, lower nitrate concentrations in both modes are predicted by HYB due to the lack of any treatment for the interaction of HNO_3 with sea salt aerosol.

Table 4 also shows that UPTAKE calculates a 70% higher fine-mode nitrate aerosol burden than DYN. Therefore, estimates of the direct aerosol forcing based on UPTAKE will be substantially overpredicted. Although HYB and DYN obtain a similar nitrate aerosol burden in the fine mode, they may still lead to different forcing estimates due to their different global aerosol distributions.

5. Conclusion and Discussion

We have implemented a hybrid dynamic approach (DYN) in a three-dimensional aerosol and chemistry model (UMICH/IMPACT) to study the global distribution of nitrate and ammonium aerosol concentrations. The DYN method is more accurate than the equilibrium model calculation and other approximate treatments for nitrate and ammonium uptake by aerosols because it includes a thermodynamic treatment of the aerosol composition which constrains the mass transport from the gas phase to coarse aerosol particles and takes account of the particle size, aerosol chemical composition, and ambient meteorological conditions in the calculation of the mass transfer rate of semi-volatile gases. Sulfate, sea salt and mineral dust aerosol are transported in the global model and aerosols are internally mixed in 4 size bins to provide reactive surfaces for heterogeneous reactions including the conversion from N_2O_5 to HNO_3 and the hydrolysis of HNO_3 and NH_3.

Results in the global model study show that 43% of the nitrate aerosol burden (0.16 Tg N) and 92% of ammonium aerosol burden (0.29 Tg N) exist in the fine aerosol mode that scatters most efficiently. 30% and 78% of the total nitrate and ammonia (gas plus aerosol) in the atmosphere is in the aerosol phase, respectively. In contrast, lower fine-mode nitrate aerosol fractions (24%) and a higher total nitrate fraction (41%) in aerosol were predicted by an offline equilibrium model calculation.

This study suggests that the formation of nitrate aerosol from HNO_3 needs to be considered in a tropospheric ozone chemistry model in addition to the HNO_3 heterogeneous conversion from N_2O_5. The presence of nitrate aerosol could enhance the tropospheric ozone decrease due to the loss of NO_x by a few percent based on our global budget analysis with larger regional changes. Nitrate aerosol has a longer lifetime than

nitric acid and is removed more efficiently by wet deposition. These differences will affect the global distribution of atmospheric nitrogen deposition, which has been indicated to be important in the global carbon cycle in the biosphere.

Sensitivity studies examined two commonly used approximations in global models for nitrate and ammonium aerosols: the UPTAKE and the HYB methods. UPTAKE and HYB significantly overpredict the uptake of nitrate by aerosols especially that by coarse particles, resulting in nitrate aerosol burdens that are higher than that in DYN by +106% and +47%, respectively. Overestimates of nitrate aerosol by HYB lead to surface HNO_3 and NO_x concentrations that are underpredicted by up to 90% and 5%, respectively, over continents. Moreover, 68% of the heterogeneous conversion of N_2O_5 to nitrate occurs on sulfate aerosol, while dust and sea salt aerosols contribute only 30% and 2%, respectively (Table 4). When sulfate aerosol is excluded, UPTAKE overpredicts the tropospheric NO_x burden by 56% and the surface NO_x concentrations by as much as a factor of 2 to 5. Sensitivity studies suggest that inaccuracies associated with the calculation of nitrate aerosol as well as differences in the form of heterogeneous reactions and aerosol types included in the model may explain the large differences in previous estimates of the decrease of tropospheric ozone due to heterogeneous interactions with aerosols, which range from 5% to 16%.

Use of the hybrid dynamical method can also improve the estimate of aerosol radiative forcing. The most recent estimate of nitrate aerosol direct forcing is that given by *Liao et al.* [2004], -0.14 Wm^{-2} for present-day nitrate aerosol. This estimate is larger than that given by *Jacobson* [2001], -0.07 Wm^{-2}, but less than that in *Adams et al.* [2001], -0.3 Wm^{-2}. *Liao et al.* [2004] improved on the two previous estimates which calculated

aerosol concentrations at thermodynamic equilibrium but they used the hybrid approach (HYB). This study shows that HYB overestimates nitrate aerosol burden in the coarse mode by more than a factor of 2 and nitrate concentrations at surface by up to a factor of 6, compared to the more accurate DYN. Excessive formation of nitrate on coarse particles can also lead to underestimates of nitrate aerosol in the fine mode, which is radiatively important. HYB therefore underestimates fine-mode nitrate by up to 50% over the surface in continents.

This study has demonstrated the importance of using the more accurate hybrid dynamical approach in the calculation of nitrate and ammonium aerosol in global aerosol and chemistry models, and has discussed the important implications for tropospheric ozone chemistry and for aerosol radiative effects. Further research into the representation of emissions, deposition, and meteorological conditions are needed to reduce the uncertainties in the calculation of aerosol nitrate and ammonium concentrations.

Acknowledgments. This work was funded by the DOE Atmospheric Chemistry Program and the NASA Atmospheric Chemistry, Modeling and Analysis Program.

TABLES

Table 1: Tropospheric Gas-phase Reactions and Heterogeneous Reactions Included in the Model

	Chemical Reactions	
Day-time Scheme [*Kraus et al*., 1996]	$NO_2 + OH + M \rightarrow HNO_3 + M$	(R1)
	$HNO_3 + h\nu \rightarrow NO_2 + OH$	(R2)
	$HNO_3 + OH \rightarrow NO_3 + H_2O$	(R3)
Night-time Scheme	$NO_2 + O_3 \rightarrow NO_3 + O_2$	(R4)
	$NO_2 + NO_3 \overset{M}{\longleftrightarrow} N_2O_5$	(R5)
Heterogeneous Interaction	$N_2O_5 + H_2O\ (a) \rightarrow 2HNO_3$	(R6)
	$NH_3 + H_2SO_4(a) = (NH_4)_2SO_4$ or NH_4HSO_4 or $(NH_4)_3H(SO_4)_2$	(R7)
	$HNO_3 + NH_3 = NH_4NO_3$	(R8)
	$HNO_3 + NaCl(a) = NaNO_3 + HCl$	(R9)
	$2HNO_3(g) + CaCO_3 = Ca(NO_3)_2 + H_2O + CO_2$	(R10)
	$2HNO_3(g) + MgCO_3 = Mg(NO_3)_2 + H_2O + CO_2$	(R11)
	$2HNO_3(g) + Na_2CO_3 = 2NaNO_3 + H_2O + CO_2$	(R12)
	$2HNO_3(g) + K_2CO_3 = 2KNO_3 + H_2O + CO_2$	(R13)

Table 2: Global Ammonia Emission by Source [*Bouwman et al*., 1997]

Source	Emission (Tg N per year)
Domesticated animals	21.6
Fertilizers	9.0
Oceans	8.2
Biomass burning	5.9
Crops	3.6
Humans	2.6
Soils under natural vegetation	2.4
Other	0.4
Total	53.6

Table 3: Comparison of Nitrate and Ammonium Global Budget with Other Studies

Budget Component	This Work	*Rodriguez and Dabdub* [2004]	*Liao et al.* [2004]	*Adams et al.* [1999]
		Burden, Tg N		
Trop. HNO_3 [a]	0.37		0.28	
Total NO_3^-	0.16	0.42	0.18	0.029
NO_3^-(D<1.25 μm)	0.067		0.059	0.029
NO_3^-(D>1.25 μm)	0.089		0.12	
NH_4^+	0.29	0.045	0.26	0.30
NH_3	0.084	0.19	0.19	0.14
		Lifetime, days		
Trop. HNO_3	4.6		3.7	
NO_3^-	5.0	7.7	4.9	
NH_4^+	4.1	3.6		4.2
NH_3	0.57	1.4		0.93
		Sources, Tg N yr^{-1}		
NO_x emission	38.9	34.7	40.0	
HNO_3 net chemical production [b]	35.8	29.7	28.1	
NO_3^- production ($HNO_3 \rightarrow NO_3^-$)	11.6	19.8	13.6	
NH_4^+ production	25.7	4.5		26.1
NH_3 emission	54.1	52.1		53.6
		Deposition, Tg N yr^{-1}		
HNO_3 dry deposition	7.5	4.0	6.3	
HNO_3 wet deposition	16.9	5.9	8.4	
NO_3^- dry deposition	3.0	1.1	7.7	
NO_3^- wet deposition	8.6	18.7	5.9	
NH_4^+ dry deposition	2.8	0.20		6.6
NH_4^+ wet deposition	23.0	4.3		19.5
NH_3 dry deposition	15.4	29.4		19.0
NH_3 wet deposition	13.1	16.7		7.4

[a] In this work, tropospheric HNO_3 burden represents for levels below 200 hPa

[b] Includes $NO_2+OH \rightarrow HNO_3$, $HNO_3+OH \rightarrow NO_3+H_2O$, $HNO_3 \rightarrow NO_2+OH$, and $N_2O_5+aerosol \rightarrow 2HNO_3$

Table 4: Comparison of the Aerosol Types Considered and Nitrate Global Budget between the Base Case and the Sensitivity Studies

	DYN (Base Case)	HYB	UPTAKE
Aerosol Types	Sulfate, Sea salt and Dust	Sulfate and Dust	Dust
	Burden (Tg N)		
NO_x (below 200 hPa, in Tg)	0.27	0.27	0.42
HNO_3 (below 200 hPa)	0.38	0.31	0.20
Total NO_3^-	0.17	0.25	0.35
NO_3^- (D<1.25 μm)	0.079	0.075	0.13
NO_3^- (D>1.25 μm)	0.086	0.18	0.22
	HNO_3 production (Tg N yr^{-1})		
NO_2 + OH	28.4	28.1	35.7
N_2O_5+aerosol	16.1	15.5	4.5
	HNO_3 loss (Tg N yr^{-1})		
HNO_3 + OH and HNO_3 + hν	5.0	4.5	4.0
Gas-to-aerosol conversion	12.6	14.8	20.7
Dry deposition	8.5	8.0	5.5
Wet deposition	17.8	16.0	10.3
	NO_3^- production (Tg N yr^{-1})		
Gas-to-aerosol (D<1.25 μm)	5.1	3.8	7.1
Gas-to-aerosol (D>1.25 μm)	7.5	11.3	13.9
	NO_3^- loss (Tg N yr^{-1})		
Dry deposition	3.5	3.3	3.2
Wet deposition	9.0	11.3	16.6

FIGURES

Figure 1. Global distribution of ammonia emissions fluxes in g N m^{-2} yr^{-1} [B*ouwman et al*., 1997] of each model grid cell.

Figure 2. Schematic diagram of the integration of the hybrid dynamical method in the global chemistry/aerosol transport model (UMICH/IMPACT).

Figure 3. Predicted monthly average mixing ratios (pptv) of nitrate aerosol in fine mode (< 1.25 μm diameter) and coarse mode (> 1.25 μm diameter) near the surface (averaged over the model lowest 3 layers), in January and July. The maximum, average and minimum values of mixing ratios are indicated above each panel.

Figure 4. Ratio of the fine-mode nitrate to total nitrate: [NO_3^- (D<1.25 μm)] / [NO_3^- (D<1.25 μm) + NO_3^- (D>1.25 μm)], near the surface in January (a) and July (b). The maximum, average and minimum values of ratios are indicated above each panel

Figure 5. Fraction of nitrate occurring as nitrate aerosol: [NO_3^-] / [NO_3^- + HNO_3(g)], near the surface in January (a) and July (b). The maximum, average and minimum values of fractions are indicated above each panel

Figure 6. Annual and zonal average HNO_3(g) and NO_3^- mixing ratios (pptv).

Figure 7. Predicted monthly average mixing ratios (pptv) of ammonium aerosol with diameter < 1.25 μm (left) and diameter > 1.25 μm (right) near the surface (averaged over the model lowest 3 layers), in January and July. The maximum, average and minimum values of mixing ratios near the surface are indicated above each panel

Figure 8. Molar ratios of ammonium aerosol to sulfate aerosol (NH_4^+/SO_4^{2-}) in the lowest 3 layers for January and July. The maximum, average and minimum values of ratios are indicated above each panel

Figure 9. Fraction of total ammonia near the surface occurring as aerosol: $[NH_4^+]$ / $[NH_4^+ + NH_3(g)]$, in January (a) and July (b). The maximum, average and minimum values of fractions are indicated above each panel

Figure 10. Annual and zonal average $NH_3(g)$ and NH_4^+ mixing ratios (pptv).

Figure 11. Schematic diagram of the global budget of nitrate and ammonium calculated in the UMICH/IMPACT model. Burdens are in Tg N and lifetimes are shown inside the boxes. Arrows indicate emissions, deposition fluxes, and net conversion rates in Tg N per year

Figure 12. Fraction of nitrate aerosol ($[NO_3^-]/[HNO_3 + NO_3^-]$) in two size ranges from an offline global thermodynamic equilibrium calculation. Numbers in parenthesis are results with sulfate aerosol only.

Figure 13. Geographic distribution of $HNO_3(g)$ and NO_x concentrations (pptv) in the lowest 3 layers of the model, calculated by DYN. Also shown are the ratios of $HNO_3(g)$ and NO_x concentrations calculated by UPTAKE and HYB over those of DYN.

Figure 14. Geographic distribution of NO_3^- concentrations (pptv) in fine mode and coarse mode calculated by DYN, and the ratio of NO_3^- concentrations between HYB and DYN in the lowest 3 layers of the model.

References

Adams, P.J., J.H. Seinfeld and D.M. Koch, Global concentrations of tropospheric sulphate, nitrate and ammonium aerosol simulated in a general circulation model, *J. Geophys. Res.*, *104*, 13791-13823, 1999.

Adams, P.J., J.H. Seinfeld, D. Koch, L. Mickley, and D. Jacob, General circulation model assessment of direct radiative forcing by the sulphate-nitrat-ammonium-water inorganic aerosol system, *J. Geophys. Res*., *106*, 1097-1111, 2001.

Balkanski, Y.J., D. J. Jacob, G. M. Gardner, W. M. Graustein, and K. K. Turekian, Transport and residence times of continental aerosols inferred from a global 3-dimensional simulation of 210 Pb, *J. Geophys. Res., 98,* 20,573–20,586, 1993.

Bauer, S.E., Y. Balkanski, M. Schulz, D. A. Hauglustaine, and F. Dentener, Global modeling of heterogeneous chemistry on mineral aerosol surfaces: Influence on tropospheric ozone chemistry and comparison to observations, *J. Geophys. Res., 109*, D02304, doi:10.1029/2003JD003868, 2004.

Bouwman, A.F., D. S. Lee, W. A. H. Asman, F. J. Dentener, K. W. Van Der HOek, and J. G. J. Olivier, A global high-resolution emission inventory for ammonia, *Global Biogeochem. Cycles, 4*, 561-587, 1997.

Capaldo, K.P., C. Pilinis and S. N. Pandis, A computationally efficient hybrid approach for dynamic gas/aerosol transfer in air quality models, *Atmos. Environ., 34,* 3617-3627, 2000.

Chin, M., D. J. Jacob, G. M. Gardner, and P. A. Spiro, A global three-dimensional model of tropospheric sulfate, *J. Geophys. Res., 101*, 18,667-18,690, 1996.

Chuang, C.C., J.E. Penner, K.E. Taylor, A.S. Grossman, and J.J. Walton, An assessment of the radiative effects of anthropogenic sulphate, *J. Geophys. Res., 102*, 3761-3778, 1997.

d'Almeida, G. A., On the variability of desert aerosol radiative characteristics, *J. Geophys. Res., 92*, 3017-3026, 1987.

Dassios, K.G., Pandis, S.N., The mass accommodation coefficient of ammonium nitrate aerosol, *Atmos. Environ., 33*, 2999-3003, 1999.

DeMore, W. B., S. P. Sander, D. M. Golden, R. F. Hampson, M. J. Kurylo, C. J. Howard, A. R. Ravishankara, C. E. Kolb, and M. J. Molina, *Chemical kinetics and photochemical data for use in stratospheric modeling*, JPL97-4, Jet Propulsion Laboratory, NASA, 1997.

Dentener, F.J., and P. J. Crutzen, Reaction of N_2O_5 on tropospheric aerosols: Impact on the global distributions of NO_x, O_3, and OH, *J. Geophys. Res., 98*, 7149-7163, 1993.

Dentener, F.J., and P. Crutzen, A three-dimensional model of the global ammonia cycle, *J. Atoms. Chem., 19*, 331-369, 1994.

Dentener, F.J., G. R. Carmichael, Y. Zhang, J. Lelieveld, and P. J. Crutzen, Role of mineral aerosol as a reactive surface in the global troposphere, *J. Geophys. Res. 101*, 22,869-22,889, 1996.

Fan, X., K. Okada, N. Niimura, K. Kai, K. Arao, G. Shi, Y. Qin, and Y. Mitsuta, Mineral particles collected in China and Japan during the same Asian dust-storm event, *Atmos. Environ., 30*, 347-351, 1996.

Feng, Y., Global Modeling of Nitrate and Ammonium Aerosol: Radiative Effect and Interaction with Gas-phase Chemistry and Aerosols, *Ph.D. thesis*, 2005.

Feng, Y., J.E. Penner, S. Sillman, X. Liu, Effects of cloud overlap in photochemical models, *J. Geophys. Res., 109,* D04310, doi:10.1029/2003JD004040, 2004.

Fuchs, N.A., and A.G. Sutugin, High dispersed aerosols, in *Topics in Current Aerosol Research (Part 2)*, Edited by G.M. Hidy and J.R. Brock, Pergamon, New York, pp 1-200, 1971.

Gerber, H. E., Relative-humidity parameterization of the Navy aerosol model (NAM), *NRL Rep.*, 8956, Natl. Res. Lab., Washington, D. C., 1985.

Gillette, D. A., E. M. Patterson Jr., J. M. Prospero, and M. L. Jackson, Soil aerosols, in *Aerosol Effects on Climate*, edited by S. G. Jennings, pp. 77-109, *Univ. of Ariz. Press*, Tucson, 1993.

Ginoux, P., M. Chin, I. Tegen, J. M. Prospero, B. Holben, O. Dubovik, andS. J. Lin, Sources and distributions of dust aerosols simulated with the GOCART model, *J. Geophys. Res., 106*, 20,255-20,273, 2001.

Giorgi, F., and W.L. Chameides, Rainout lifetimes of highly soluble aerosols and gases as inferred from simulations with a general circulation model, *J. Geophys. Res.*, *91*, 14,367-14,376, 1986.

Gong, S. L., L. A. Barrie, J. M. Prospero, D. L. Savoie, G. P. Ayers, J. P. Blanchet, and L. Spacek, Modeling sea-salt aerosols in the atmosphere: 2. Atmospheric concentrations and fluxes, *J. Geophys. Res., 102*, 3819-3830, 1997.

Goodman, A.L., G. M. Underwood, and V. H. Grassian, A laboratory study of the heterogeneous reaction of nitric acid on calcium carbonate particles, *J. Geophys. Res., 105*, 29,053-29,064, 2000.

IPCC (Intergovernmental Panel on Climate Change), Radiative Forcing of Climate Change and an Evaluation of the IPCC IS92 Emission Scenarios, edited by Houghton, J.T., L.G. Meira Filho, J. Bruce, H. Lee, B.A. Callander, E.F. Haites, N. Harris, and K. Maskell, *Cambridge University Press*, Cambridge, United Kingdom and New York, NY, USA, 1994.

Ito, A., J.E. Penner, and S. Sillman, AGU fall meeting, 2004.

Jacob, D.J., Heterogeneous chemistry and tropospheric ozone, *Atmos. Environ., 34*, 2131-2159, 2000.

Jacob, D.J., and S. C. Wofsy, Budgets of reactive nitrogen, hydrocarbons, and ozone over the Amazon forest during the wet season, *J. Geophys. Res., 95*, 16,737-16,754, 1990.

Jacobson, M.Z., Studying the effects of calcium and magnesium on size-distributed nitrate and ammonium with EQUISOLV II, *Atmos. Environ., 33*, 3635-3649, 1999.

Jacobson, M.Z., Global direct radiative forcing due to multicomponent anthropogenic and natural aerosols, *J. Geophys. Res., 106(D2)*, 1551-1568, 2001.

Jaenicke, R., landolt-Bornstein Zahlenwerte und Funktionen aus Naturwissenschaften und Technik, 4, Meteorologie, B, *Physikalishe und Chemische Eigenschaften der Luft*, 391-457, Springer, New York, 1988.

John, W., S.M. Wall, J.L. Ondo, and W. Winklmayr, Acidic-aerosol size distributions during SCAQS (Southern California Air Quality Study), Final report, 1989.

Kerminen, V.M., T.A. Pakkanen, and R.E. Hillamo, Interactions between inorganic trace gases and supermicrometer particles at a coastal site, *Atmos. Environ., 31*, 2753-2765, 1997.

Kraus, A.B., F. Rohrer, E.S. Grobler, and D.H. Ehhalt, The global tropospheric distribution of NO_x estimated by a three-dimensional chemical tracer model, *J. Geophys. Res., 101*(D13), 18,587-18,604, 1996.

Kulmula, M., A. Laaksonen, P. Korhonen, T. Vesala and T. Ahonen, The effect of atmospheric nitric acid vapor on cloud condensation nucleus activation, *J. Geophys. Res., 98*, 22949-22958, 1993.

Kulmala, M., P. Korhonen, A. Laaksonen, and T. Vesala, Changes in cloud properties due to NOx emissions, *Geophys. Res. Lett., 22*, 239-242, 1995.

Kulmala,M., A. Toivonen, T. Mattila, and P. Korhonen, Variations of cloud droplet concentrations and the optical properties of clouds due to changing hygroscopicity: A model study, *J. Geophys. Res., 103*, 16183-16195, 1998.

Lelieveld, J., G.J. Roelofs, L. Ganzeveld, J. Feichter, and H. Rodhe, Terrestrial sources and distribution of atmospheric sulphur, *Phil. Trans. R. Soc. Lond. B., 352*, 149-158, 1997.

Liao, H., P. J. Adams, S. H. Chung, J. H. Seinfeld, L. J. Mickley, and D. J. Jacob, Interactions between tropospheric chemistry and aerosols in a unified general circulation model, *J. Geophys. Res., 108(D1)*, 4001, doi:10.1029/2001JD001260, 2003.

Liao, H., J. H. Seinfeld, P. J. Adams, and L. J. Mickley, Global radiative forcing of coupled tropospheric ozone and aerosols in a unified general circulation model, *J. Geophys. Res., 109*, D16207, doi:10.1029/2003JD004456, 2004.

Liu, H., D. J. Jacob, I. Bey, and R. M. Yantosca, Constraints from ^{210}Pb and ^{7}Be on wet deposition and transport in a global three-dimensional chemical tracer model driven by assimilated meteorological fields, *J. Geophys. Res.*, *106*(D11), 12109-12128, 2001.

Liu, X. and J.E. Penner, Effect of Mount Pinatubo H_2SO_4/H_2O aerosol on ice nucleation in the upper troposphere using a global chemistry and transport model, *J. Geophys. Res., 107(D12),* 4141, doi:10.1029/2001JD000455, 2002.

Liu, X., J.E. Penner, and M. Herzog, Global modeling of aerosol dynamics: Model description, evaluations, and interactions between sulfate and nonsulfate aerosols, submitted to *J. Geophys. Res.*, 2005.

Lurmann, F.W., A.S. Wexler, S.N. Pandis, S. Musarra, N. Kumar, and J. H. Seinfeld, Modeling urban and regional aerosols, II, Application to California's south coast air basin, *Atmos. Environ. 31*, 2695-2715, 1997.

Mari, C., D. J. Jacob, and P. Bechtold, Transport and scavenging of soluble gases in a deep convective cloud, *J. Geophys. Res.*, *105*(D17), 22,255-22,268, 2000.

Meng, Z., and J. H. Seinfeld, Time scales to achieve atmospheric gas-aerosol equilibrium for volatile species, *Atmos. Environ., 30*, 2889-2900, 1996.

Metzger, S., F. Dentener, M. Krol, A. Jeuken, and J. Lelieveld, Gas/aerosol partitioning: 2. Global modeling results, *J. Geophys. Res., 107(D16)*, 4313, doi:10.1029/2001JD001103, 2002.

Monahan, E. C., D. E. Spiel, and K. L. Davidson, A model of marine aerosol generation via whitecaps and wave disruption, in *Oceanic Whitecaps and Their Role in Air-Sea Exchange*, edited by E. C. Monahan and G. MacNiocaill, pp. 167-174, D. Reidel, Norwell, Mass., 1986.

Niimura, N., K. Okada, X. Fan, K. Kai, K. Arao, G. Y. Shi, and S. Takahashi, Formation of Asian dust-storm particles mixed internally with sea salt in the atmosphere, *J. Meteorol. Soc. Jpn., 76*, 275-288, 1998.

Okada, K., H. Naruse, T. Tanaka, O. Nemoto, Y. Iwasaka, P. Wu, A. Ono, R. Duce, M. Uematsu, and J. Merrill, X-ray spectrometry of individual Asian dust-storm particles over the Japanese Islands and the North Pacific Ocean, *Atmos. Environ., Part A, 24*, 1369-1378, 1990.

Pandis, S.N., A. S. Wexler, and J. H. Seinfeld, Secondary organic aerosol formation and transport, II, Predicting the ambient secondary organic aerosol size distribution, *Atmos. Environ., 27A*, 2403-2416, 1993.

Penner, J.E., C. A. Atherton, and T. E. Graedel, Global emissions and models of photochemically active compounds, in *Global Atmospheric-Biospheric Chemistry*, edited by R. Prinn, pp. 223-248, Plenum, New York, 1994.

Penner, J.E., C.C. Chuang and K. Grant, Climate forcing by carbonaceous and sulphate aerosols, *Clim. Dyn., 14*, 839-851, 1998.

Penner, J.E., M. Andreae, H. Annegarn, L. Barrie, J. Feichter, D. Hegg, A. Jayaraman, R. Leaitch, D. Murphy, J. Nganga, and G. Pitari, Aerosols, their Direct and Indirect Effects, in *Climate Change 2001: The Scientific Basis*, Ed. by H. T. Houghton, Y. Ding, D. J. Griggs, M. Noguer, P. J. van der Linden, X. Dai, K. Maskell, C. A. Johnson, *Report to Intergovernmental Panel on Climate Change from the Scientific Assessment Working Group (WGI)*, Cambridge University Press, 289-416, 2001.

Quinn, P.K., D.J. Coffman, V.N. Kapustin, T.S. Bates and D.S. Covert, Aerosol optical properties in the marine boundary layer during the First Aerosol Characterization Experiment (ACE 1) and the underlying chemical and physical aerosol properties, *J. Geophys. Res., 103*, 16,547-16,563, 1998.

Riemer, N., H. Vogel, B. Vogel, B. Schell, I. Ackermann, C. Kessler, and H. Hass, Impact of the heterogeneous hydrolysis of N2O5 on chemistry and nitrate aerosol formation in the lower troposphere under photomog conditions, *J. Geophys. Res., 108*(D4), 4144, doi:10.1029/2002JD002436, 2003.

Rodriguez, M. A., and D. Dabdub, IMAGES-SCAPE2: A modeling study of size- and chemically resolved aerosol thermodynamics in a global chemical transport model, *J. Geophys. Res., 109*, D02203, doi:10.1029/2003JD003639, 2004.

Roeckner, E., T. Siebert, and J. Feichter, Climatic response to anthropogenic sulfate forcing simulated with a general circulation model, in *Aerosol Forcing of Climate* [Charlson, R. and J. Heintzenberg (eds.)], John Wiley and Sons, pp. 349-362, 1994.

Rotman D. A., C.S. Atherton, D.J. Bergmann, P.J. Cameron-Smith, C.C. Chuang, P.S. Connell, J.E. Dignon, A. Franz, K.E. Grant, D.E. Kinnison, C.R. Molenkamp, D.D. Proctor, and J.R. Tannahill, IMPACT, the LLNL 3-D global atmospheric chemical transport model for the combined troposphere and stratosphere: Model description and analysis of ozone and other trace gases, *J. Geophys. Res., 109*, D04303, doi:10.1029/2002JD003155, 2004.

Saxena, P. and L.M. Hildemann, Water soluble organics in atmospheric particles: A critical review of the literature and application of thermodynamics to identify candidate compounds, *J. Atmos. Chem., 24*, 57-109, 1996.

Schlesinger, W. H., and A. E. Hartley, A global budget for atmospheric NH_3, *Biochem., 15*, 191-211, 1992.

Schultz, M.G., D.J. Jacob, Y. Wang, J.A. Logan, E.L. Atlas, D.R. Blake, N.J. Blake, J.D. Bradshaw, E.V. Browell, M.A. Fenn, F. Flocke, G.L. Gregory, B.G. Heikes, G.W. Saches, S.T. Sandholm, R.E. Shetter, H.B. Singh, and R.W. Talbot, On the origin of

tropospheric ozone and NO_x over the tropical South Pacific, *J. Geophys. Res., 104*, 5829-5844, 1999.

Seinfeld, J.H. and S.N. Pandis, Atmospheric Chemistry and Physics: From Air Pollution to Climate Change, *John Wiley and Sons*, New York, 1998.

Singh, H.B., W. Viezee, Y. Chen, A.N. Thakur, Y. Kondo, R.W. Talbot, G.L. Gregory, G.W. Sachse, D.R. Blake, J.D. Bradshaw, Y. Wang, and D.J. Jacob, Latitudinal distribution of reactive nitrogen in the free troposphere over the Pacific Ocean in late winter/early spring, *J. Geophys. Res., 103*, 28,237-28,247, 1998.

Singh, H., Y. Chen, A. Tabazadeh, Y. Fukui, I. Bey, R. Yantosca, D. Jacob, F. Arnold, K. Wohlfrom, E. Atlas, F. Flocke, D. Blake, N. Blake, B. Heikes, J. Snow, R. Talbot, G. Gregory, G. Sachse, S. Vay, and Y. Kondo, Distribution and fate of selected oxygenated organic species in the troposphere and lower stratosphere over the Atlantic, *J. Geophys. Res., 105*, 3795-3806, 2000.

Schwartz, S.E., Mass transport considerations pertinent to aqueous-phase reactions of gases in liquid-water clouds, in *Chemistry of Multiphase Atmospheric Systems*, edited by W. Jaeschke. Springer-Verlag, Berlin, pp. 415-471.

Tang, I.N., and H.R. Munkelwitz, Water activities, densities, and refractive indices of aqueous sulfate and sodium nitrate droplets of atmospheric importance, *J. Geophys. Res., 99*, 18,801-18,808, 1994.

Takemura, T., H. Okamoto, Y. Maruyama, A. Numaguti, A. Higurashi, and T. Nakajima, Global three-dimensional simulation of aerosol optical thickness distribution of various origins, *J. Geophys. Res., 105*, 17,853-17,873, 2000.

Tegen, I., S. P. Harrison, K. Kohfeld, I. C. Prentice, M. Coe, and M. Heimann, Impact of vegetation and preferential source areas on global dust aerosol: Results from a model study, *J. Geophys. Res., 107*(D21), 4576, doi:10.1029/2001JD000963, 2002.

ten Brink, H.M., J. P. Veefkind, A. Waijers-Ijpelaan, and J. C. van der Hage, Aerosol light-scattering in the Netherlands, *Atmos. Environ., 30*, 4251-4261, 1996.

ten Brink, H.M., C. Kruisz, G.P.A. Kos, and A. Berner, Composition/size of the light-scattering aerosol in the Netherlands, *Atmos. Environ., 31*, 3955-3962, 1997.

Tie, X., L. Emmons, L. Horowitz, G. Brasseur, B. Ridley, E. Atlas, C. Stround, P. Hess, A. Klonecki, S. Madronich, R. Talbot, and J. Dibb, Effect of sulfate aerosol on tropospheric NO_x and ozone budgets: Model simulations and TOPSE evidence, *J. Geophys. Res., 108*, 8364, doi: 10.1029/2001JD001508, 2003.

Van Doren , J.M., L.R. Watson, P. Davidovits, D.R.. Worsnop, M.S. Zahniser and C.E. Kolb, Temperature Dependence of the Uptake Coefficient of HNO_3, HCl and N_2O_5 on Water Droplets, *J. Phys. Chem., 94*, 3265-3269, 1990.

Van Doren , J.M., L. R. Watson, P. Davidovits, D. R. Worsnop, M. S. Zahniser, and C. E. Kolb, Uptake of N_2O_5 and HNO_3 on Aqueous Sulfuric Acid Droplets as a Function of Sulfuric Acid Concentration: Coefficients and Branching Ratio, *J. Phys. Chem., 95*, 1684-1689, 1991.

Van Dorland, R., F.J. Dentener and J. Lelieveld, Radiative forcing due to tropospheric ozone and sulphate aerosols, *J. Geophys. Res., 102*, 28,079-28,100, 1997.

Walcek, C.J., R.A. Brost and J.S. Chang, SO_2, sulfate and HNO_3 deposition velocities computed using regional landuse and meteorological data, *Atmos. Environ., 20*, 949-964, 1986.

Warneck, P., Chemistry of the natural atmosphere, 757pp., *Academic*, San Diego, Calif., 1988.

Wesely, M.L., Parameterization of surface resistances to gaseous dry deposition in regional-scale numerical models, *Atmos. Environ., 23*, 1293-1304, 1989.

Wexler, A. S., and J. H. Seinfeld, The distribution of ammonium salts among a size and composition dispersed aerosol, *Atmos. Environ., Part A, 24*, 1231-1246, 1990.

Williamson, D.L., J.T. Kiehl, V. Ramanathan, R.E. Dickinson, J.J. Hack, Description of NCAR Community Climate Model (CCM1), *NCAR Technical Note*, NCAR/TN-285+STR, 112 pp., 1987.

Wu, P.M., and K. Okada, Nature of coase nitrate particles in the atmosphere - a single particle approach, *Atmos. Environ., 28*, 2053-2060, 1994.

Yeatman, S.G., L.J. Spokes, and T.D. Jickells, Comparisons of coarse-mode aerosol nitrate and ammonium at two polluted coastal sites, *Atmos. Environ., 35*, 1321-1335, 2001.

Yamato, Y. and H. Tanaka, Aircraft observations of aerosols in the free marine troposphere over the North Pacific Ocean: Particle chemistry in relation to air mass origin, *J. Geophys. Res., 99*, 5353-5377, 1994.

Zhang, D., Y. Iwasaka, G. Shi, J. Zang, A. Matsuki, and D. Trochkine, Mixture state and size of Asian dust particles collected at southwestern Japan in spring 2000, *J. Geophys. Res., 108(D24)*, 4760, doi:10.1029/2003JD003869, 2003.

Zhang, L., S.L. Gong, J. Padro, and L. Barrie, A size-segregated particle dry deposition scheme for an atmospheric aerosol module, *Atmos. Environ., 35 (3)*, 549-560, 2001.

Zhou, M., K. Okada, F. Qian, P.-M. Wu, L. Su, B. E. Casareto, and T. Shimohara, Characteristics of dust-storm particles and their long-range transport from China to Japan-Case studies in April 1993, *Atmos. Res., 40*, 19-31, 1996.

Zhuang, H., C.K. Chan, M. Fang, and A.S. Wexler, Formation of nitrate and non-sea salt sulfate on coarse particles, *Atmos. Environ., 33*, 4223-4233, 1999.

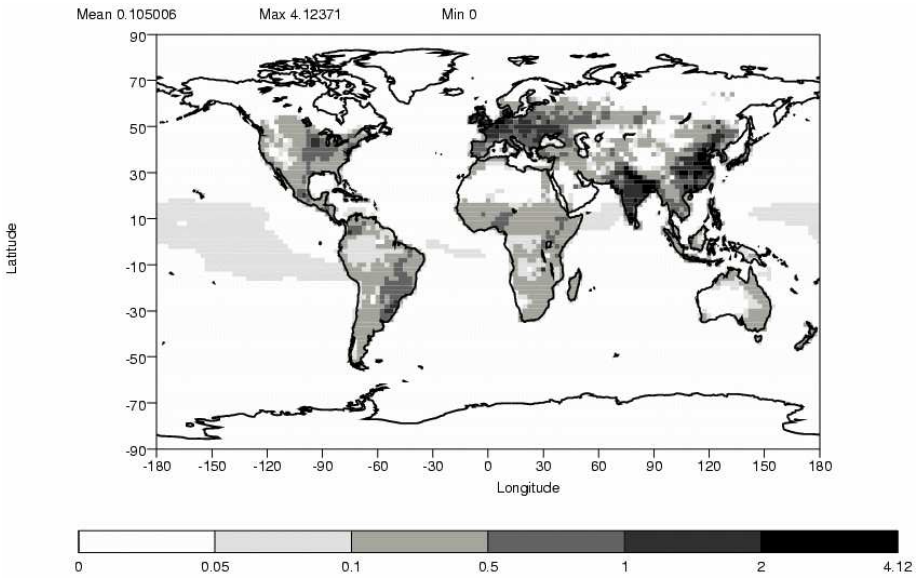

Figure 1: Global distribution of ammonia emissions fluxes in g N m^{-2} yr^{-1} [*Bouwman et al.*, 1997] of each model grid cell.

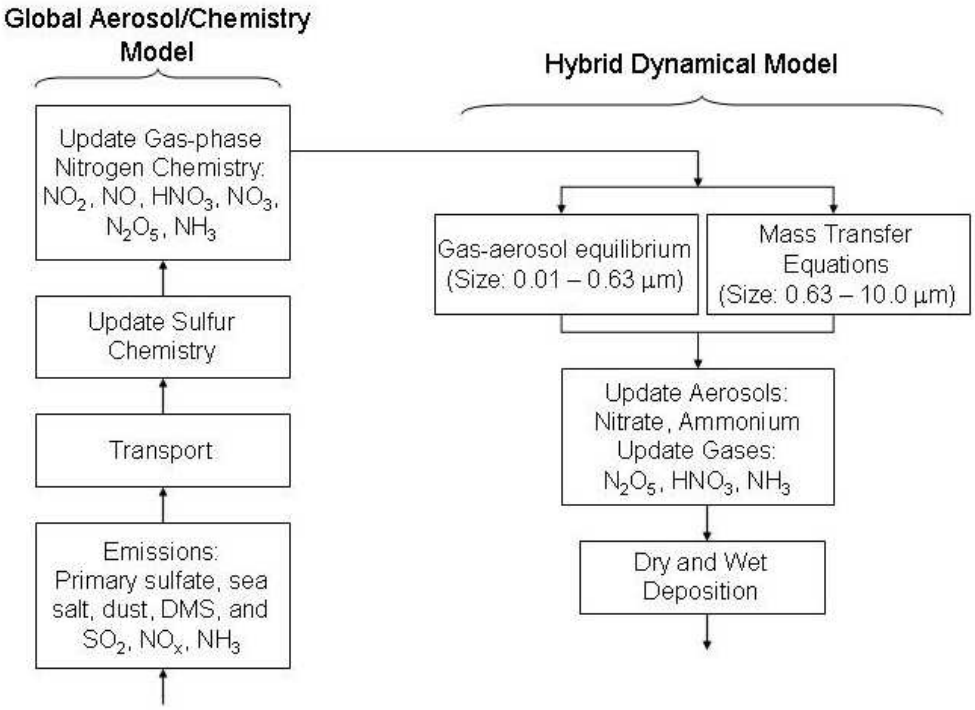

Figure 2: Schematic diagram of the integration of the hybrid dynamical method in the global chemistry/aerosol transport model (UMICH/IMPACT).

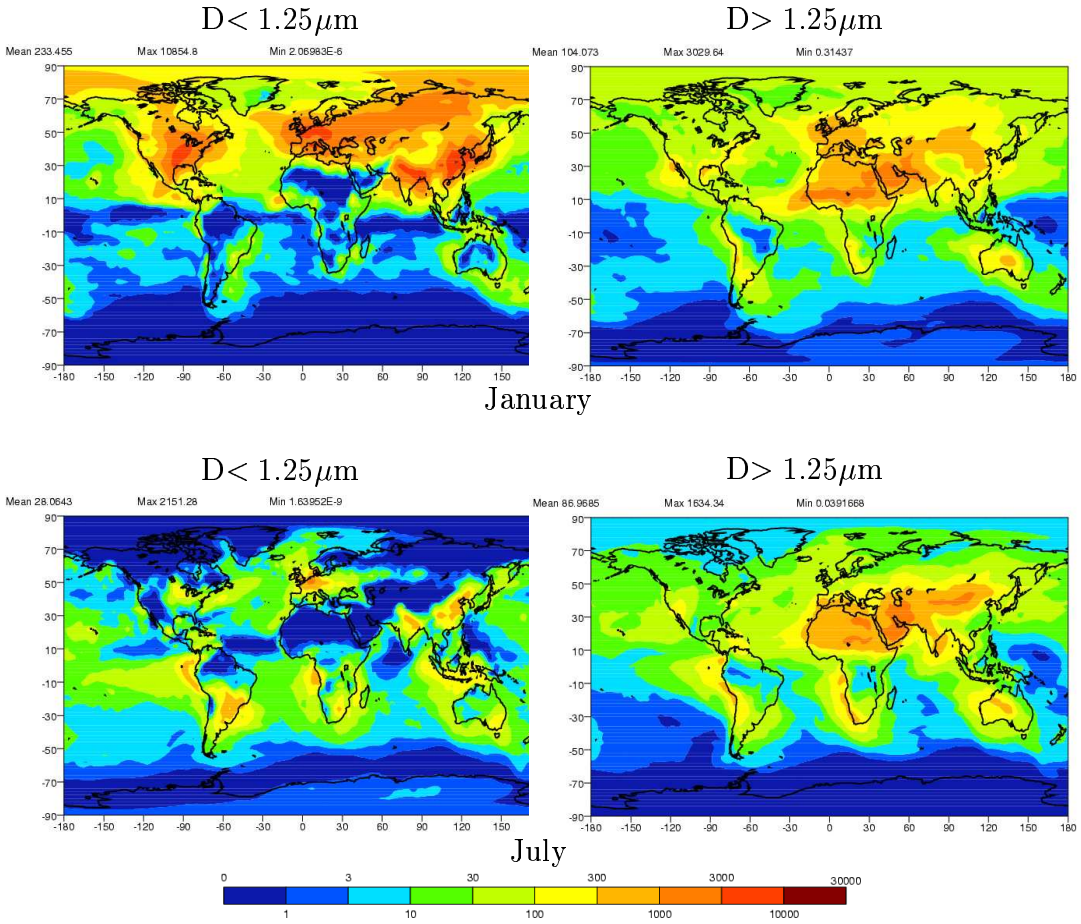

Figure 3: Predicted monthly average mixing ratios (pptv) of nitrate aerosol in fine mode ($< 1.25\mu$m diameter) and coarse mode ($> 1.25\mu$m diameter) near the surface (averaged over the model lowest 3 layers), in January and July. The maximum, average and minimum values of mixing ratios are indicated above each panel.

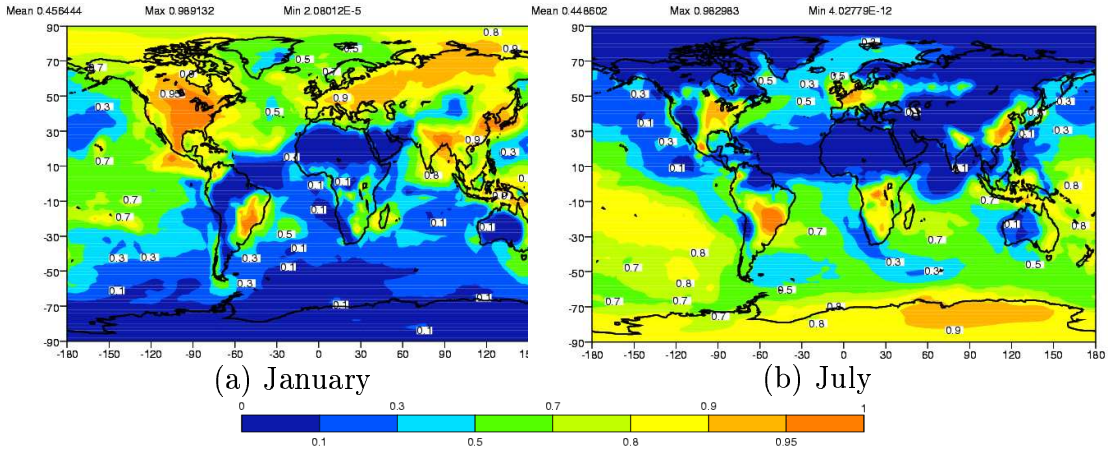

Figure 4: Ratio of the fine-mode nitrate to total nitrate: $[NO_3^-$ (D$<1.25\mu$m)] / [NO_3^- (D$<1.25\mu$m) + NO_3^- (D$>1.25\mu$m)], near the surface in January (a) and July (b). The maximum, average and minimum fractions are indicated above each panel.

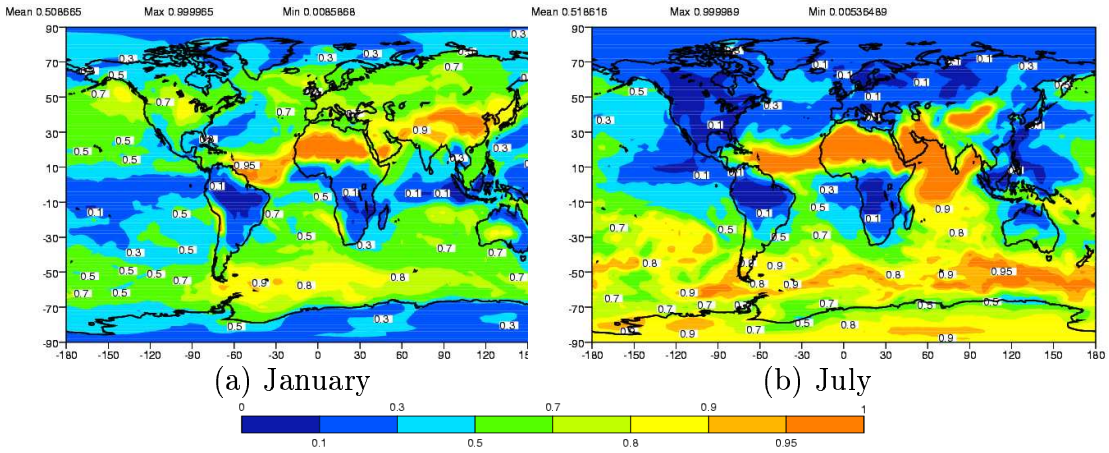

Figure 5: Fraction of nitrate occurring as nitrate aerosol: $[NO_3^-]$ /[NO_3^- + HNO_3(g)], near the surface in January (a) and July (b). The maximum, average and minimum values of fractions are indicated above each panel.

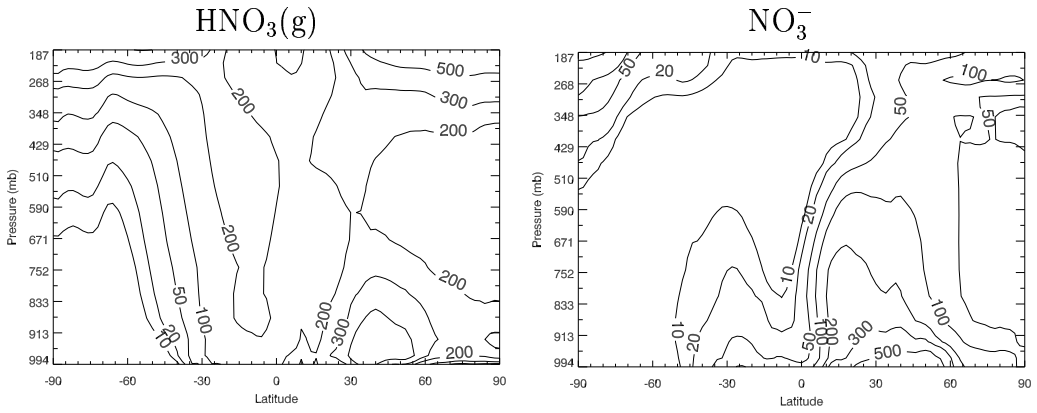

Figure 6: Annual and zonal average $HNO_3(g)$ and NO_3^- mixing ratios (pptv).

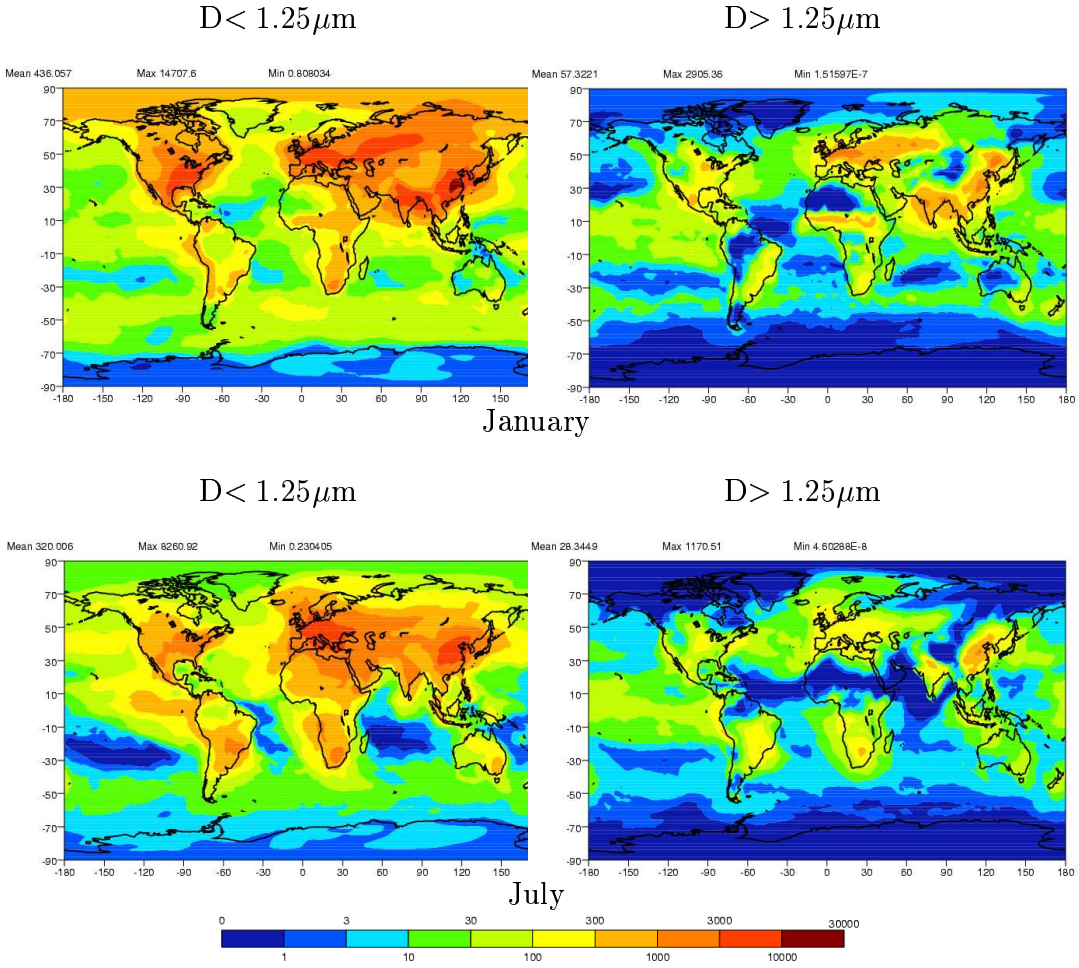

Figure 7: Predicted monthly average mixing ratio (pptv) of ammonium aerosol with diameter $< 1.25\mu$m and diameter $> 1.25\mu$m near the surface (averaged over the model lowest 3 layers), in January and July. The maximum, average and minimum values of mixing ratios are indicated above each panel.

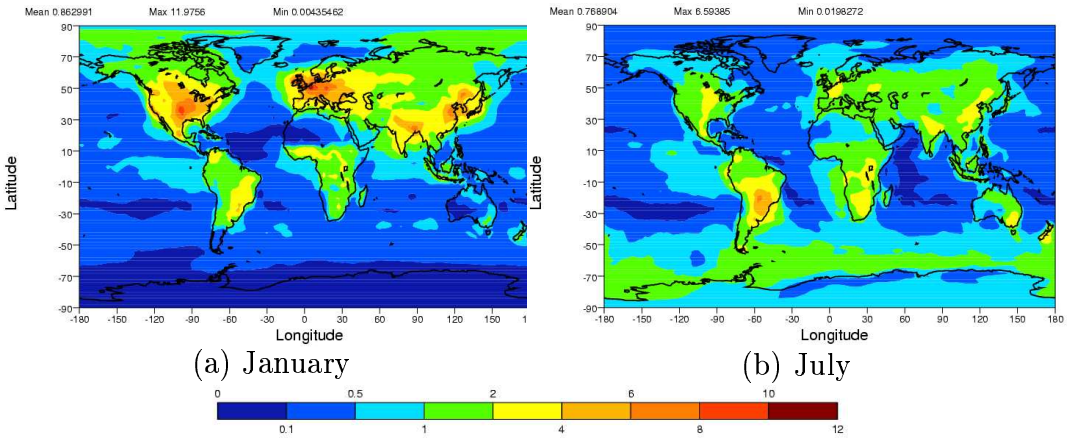

Figure 8: Molar ratios of ammonium aerosol to sulfate aerosol (NH_4^+/SO_4^{2-}) in the lowest 3 layers for January and July. The maximum, average and minimum values of ratios are indicated above each panel.

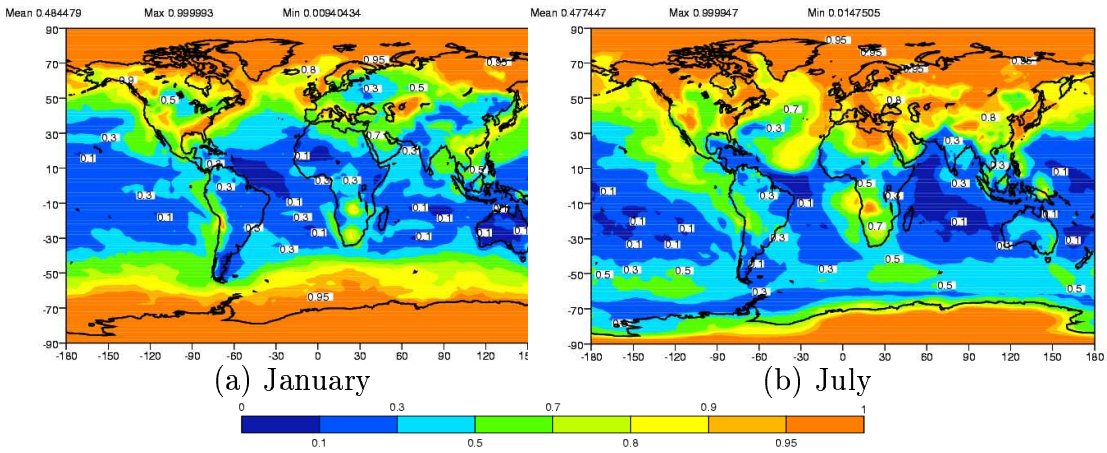

Figure 9: Fraction of total ammonia near the surface occurring as aerosol: $[NH_4^+]\ /[NH_4^+ + NH_3(g)]$, in January (a) and July (b). The maximum, average and minimum values of fractions are indicated above each panel.

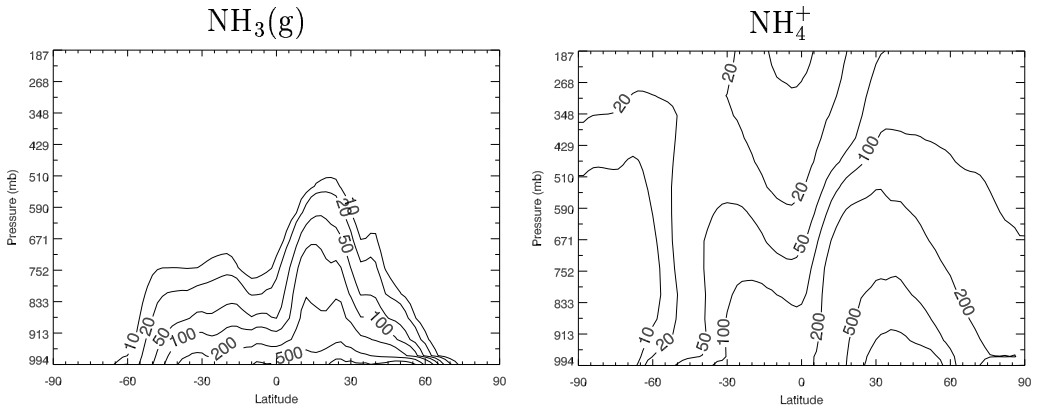

Figure 10: Annual and zonal average $NH_3(g)$ and NH_4^+ mixing ratios (pptv).

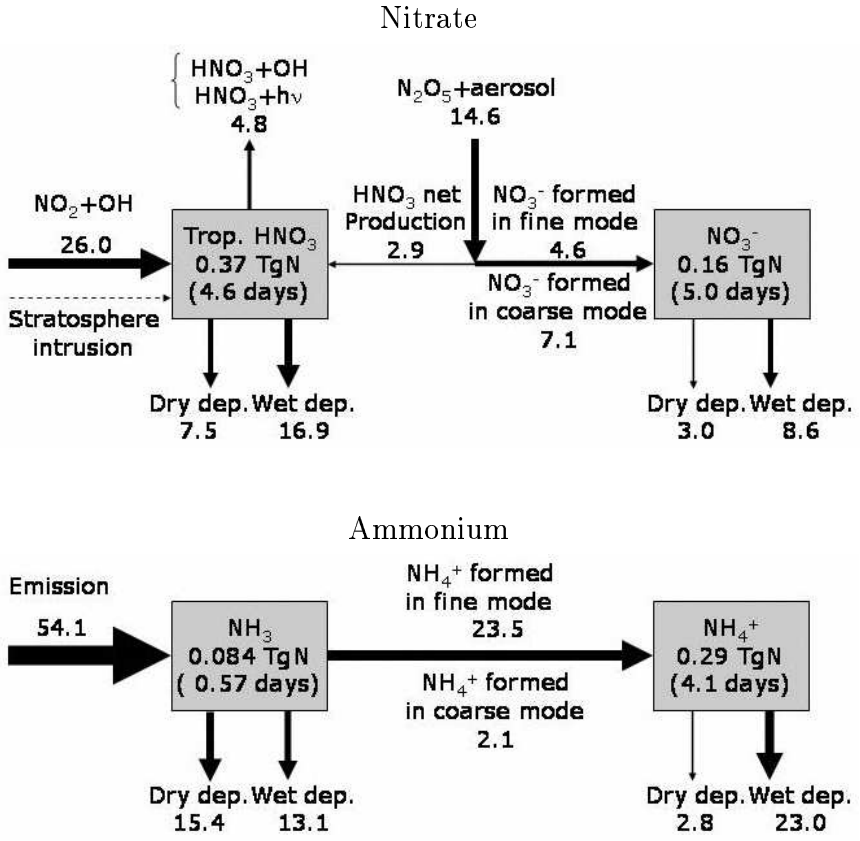

Figure 11: Schematic diagram of the global budget of nitrate and ammonium aerosol calculated in the UMICH/IMPACT model. Burdens are in Tg N and lifetimes are shown inside the boxes. Arrows indicate emissions, deposition fluxes, and net conversion rates in Tg N yr^{-1}.

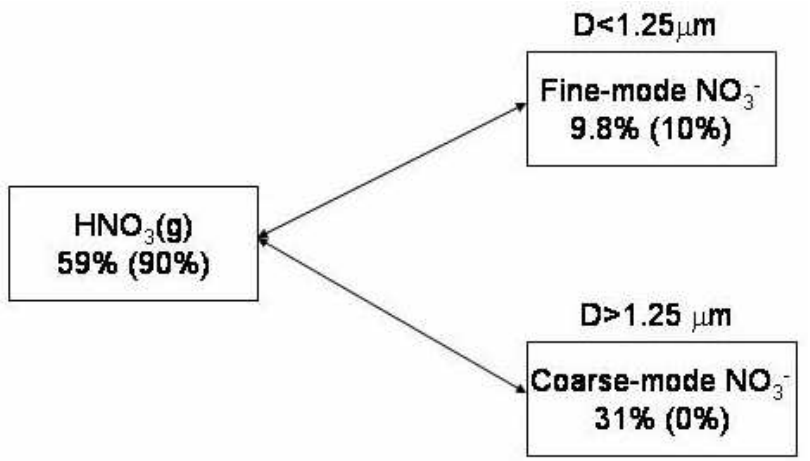

Figure 12: Fraction of nitrate aerosol ($[NO_3^-]$ / $[HNO_3(g) + NO_3^-]$) in two size ranges from an offline global thermodynamic equilibrium calculation. Numbers in parenthesis are results with sulfate aerosol only.

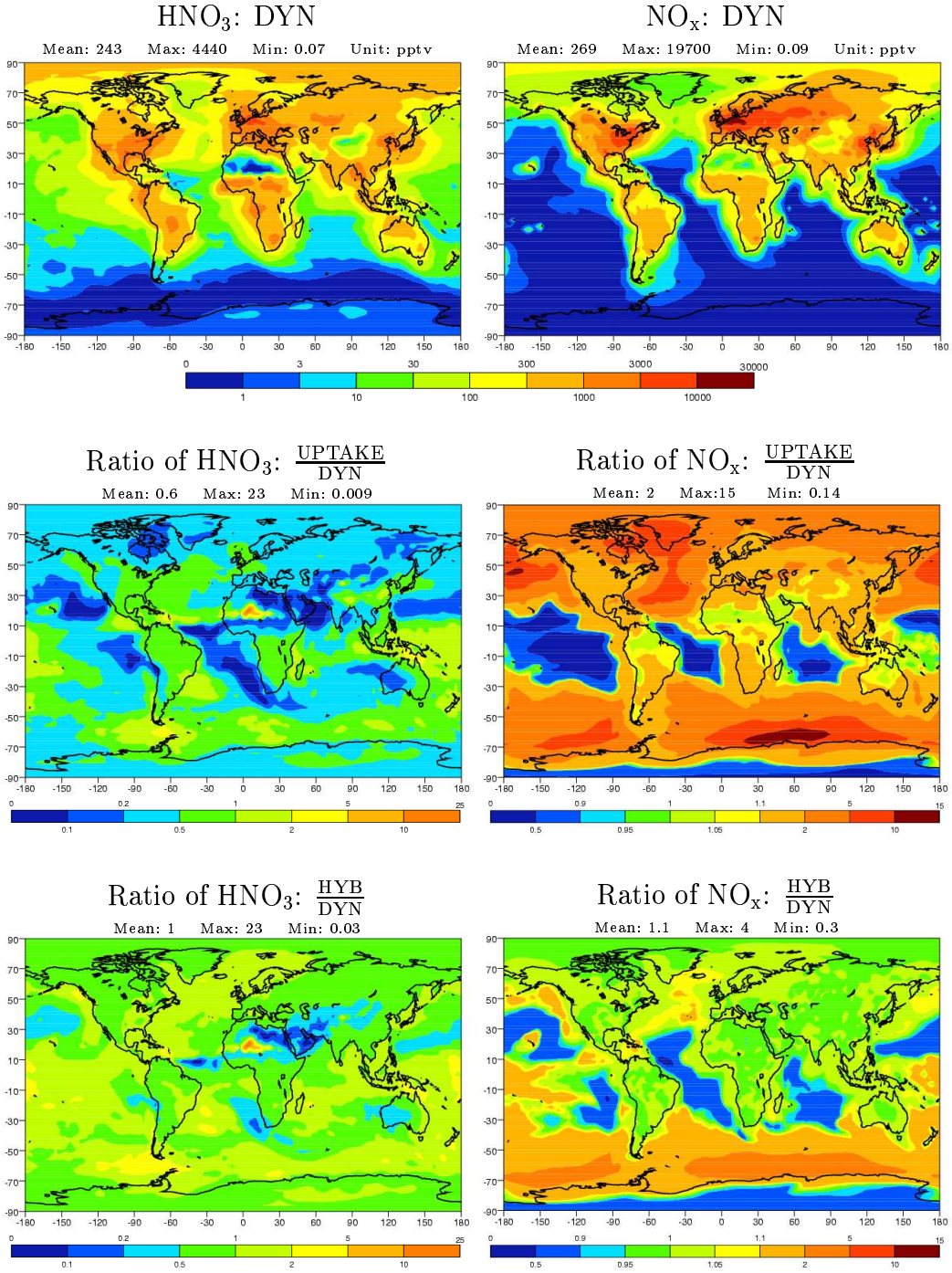

Figure 13: Geographic distribution of HNO_3(g) and NO_x concentrations in the lowest 3 layers of the model, calculated by DYN. Also shown are the ratios of HNO_3(g) and NO_x concentrations calculated by UPTAKE and HYB over that of DYN.

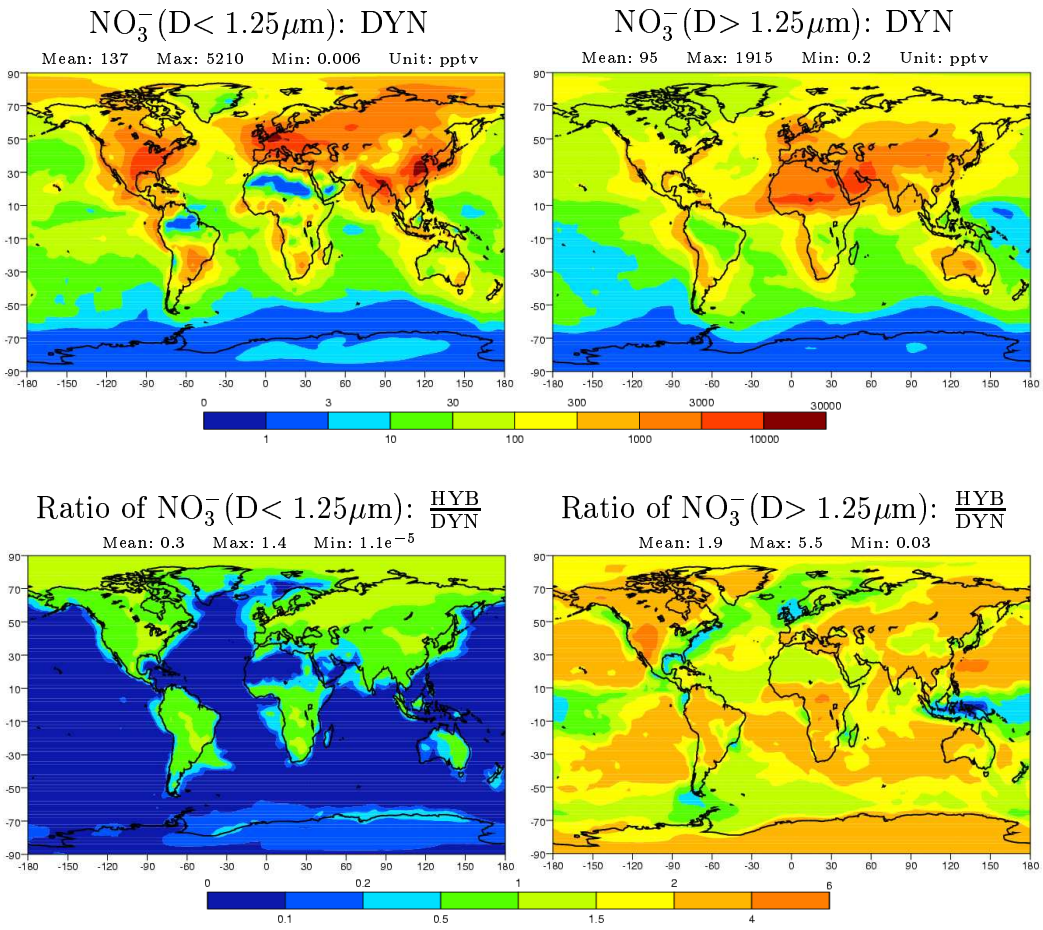

Figure 14: Geographic distribution of NO_3^- concentrations (pptv) in fine mode and coarse mode calculated by DYN, and the ratio of NO_3^- concentrations between HYB and DYN in the lowest 3 layers of the model.